Recent advances on electrospun nanofiber materials for post-lithium ion batteries

Fangyi Shi[a,b] , Chunhong Chen[a], Zheng-Long Xu[a*]

[a] Department of Industrial and Systems Engineering, the Hong Kong Polytechnic University, Hung Hom, Hong Kong, P.R. China

[b] Department of Applied Physics, The Hong Kong Polytechnic University, Hung Hom, Hong Kong, P.R. China

*Corresponding author: ZL Xu Email: zhenglong.xu@polyu.edu.hk

Abstract

Lithium ion batteries (LIBs) have dominated the portable electric market over decades; however, the limited and unevenly distributed lithium resources induce concerns on their future large-scale applications. Increasing efforts have been endeavored on exploring post-Li ion batteries, such as Na-ion, K-ion, Al-ion and Mg-ion batteries, due to the high abundance of the corresponding elements in Earth crust. Manufacturing reliable electrode materials is the key to develop these new battery systems. Facile and scalable electrospinning has been widely utilized in preparing mechanically stable, flexible and conductive nanofiber electrodes as successfully proven in LIBs. In recent years, tremendous efforts have been devoted to electrospinning nanofiber electrodes for post-Li ion batteries and discernible progress in the electrochemical performance has been witnessed. Herein, we aim to review the-state-of-the-art advances made in electrospun nanofiber materials in optimizing post-Li ion battery technology by surveying the correlations among the morphology, the surface chemistry, the structure of electrospun nanofibers, and the post-Li ion batteries performance. Based on intensive investigations and insightful understandings, perspectives to the future design of electrospun nanofiber electrodes are also presented.

Keywords: Electrospinning, nanofibers, electrodes, post-Li ion batteries

1. Introduction

There are increasing demands for renewable energy to replace traditional fossil fuels (such as coal, oil) for the sustainable development of the society [1, 2]. Solar and wind powers are regarded as clean energy sources; however, their intermittent nature requires energy storage systems to guarantee the continuous power supply. Rechargeable batteries based on electrochemical energy storage are one of the most promising candidates to solve this challenge because of their high energy densities, high design flexibility, and large manufacturing capability. Since the successful launch of lithium ion batteries (LIBs) in 1990s, they have become the common choice to power portable electronic devices such as smartphones and laptops [3, 4]. The great success of LIBs in small electrics has also encouraged them to penetrate into electric vehicle and smart grid markets. However, the large-scale application of LIBs inevitably raises concerns about the cost and availability of LIBs and lithium resources. Lithium is identified as a scarce element (20 ppm) and unevenly distributed in Earth crust [5]. The rapid increment in LIBs consumption also invoked the recent leap in the cost of lithium carbonate [6]. Thus, concerns about limited lithium resources should not be overlooked. In addition, the LIBs with energy densities of 100-260 Wh kg^{-1} are insufficient to meet the requirements for the long driving electric vehicles [4, 7, 8]. Therefore, exploring post-Li ion battery technologies with higher energy density, lower cost and higher availability becomes imperative.

Among the few post-Li ion batteries candidates, lithium-sulfur batteries (LSBs) are considered promising to induce breakthrough in energy density due to their high theoretical energy density of 2600Wh kg^{-1} and low-cost of sulfur feedstock. Nevertheless, the implementation of LSBs is stalled by several fundamental challenges, including the insulating nature of sulfur and lithium sulfides, the shuttling effect of long-chain polysulfides and the large volume

expansion/contraction of sulfur during discharge/charge processes, leading to fast capacity degradation and poor rate performance [9, 10]. Among the many strategies to mitigate the above challenges, electrospun nanofibers have played effective roles, to be discussed later. On the other hand, compared to lithium, other alkaline and alkali metal elements, including sodium (Na), potassium(K), magnesium (Mg), aluminum (Al), and zinc (Zn), are much more abundant inon the Earth crust (*i.e*., 23600 ppm for Na, 20900 ppm for K, 950 ppm for Mg, and 82300 ppm for Al, **Table 1**) [11], potentially leading to lower cost and more available rechargeable batteries for large-scale energy applications. Na-ion batteries (SIBs) and K-ion batteries (PIBs) share the similar working principles to LIBs that Na or K ions are transported between anode and cathode materials to store and release the electrochemical energy reversibly [12]. The differences mainly lie in the larger radius sizes (1.02 Å for Na^+, 1.38 Å for K^+ versus 0.76 Å for Li^+) and the higher standard electrode potentials (-2.71 V *vs*. standard hydrogen electrode (SHE) for Na^+/Na, -2.93 V vs. SHE for K^+/K versus -3.04 V vs. SHE for Li^+/Li) for Na^+ and K^+, which may lead to lower specific capacities and lower energy densities for SIBs and KIBs than LIBs. In addition, the large ionic radius sizes also induce huge volume variations for electrode materials during the cycling of SIBs and KIBs, resulting in short cycle life. To overcome these obstacles, smart nanostructures have been designed with the assistance of electrospinning to be discussed later.

For multivalent-ion (Mg^{2+}, Zn^{2+}, and Al^{3+}) batteries, they have the potential to bring about energy breakthrough than that for monovalent ion batteries by associating with double or triple electron transfer per charge carrier. In addition, Al and Mg metal anodes are considered dendrite-free during deposition [12], which indicates the long-awaited metal battery systems with high safety. However, the development of multivalent-ion batteries has been stalled by the slow diffusion kinetics of multivalent ions in electrolyte and electrodes, the lack of stable electrodes and

the formation of unstable solid electrolyte interface. To overcome these challenges, active particles have been incorporated into electrospun carbon nanofibers, to take advantage of the high conductivity, large surface area, and high porosity of nanofibrous structures. Hitherto, significant progress in electrochemical performance has been obtained for electrospun electrodes in multivalent ion batteries.

It is clear that post-Li ion batteries possess unique advantages compare to conventional LIBs for next-generation energy storage applications, whose development depends on the smart design of battery components[7, 12]. For electrode materials, nanostructure materials generally exhibit superior stability and faster kinetics than their bulk counterparts, due to the high tolerance to fracture and amplified electrolyte/electrode interface [13]. On the base of dimensions, nanomaterials can be grouped into zero-dimensional (0D) nanoparticles, one-dimensional (1D) nanotubes or nanofibers, two-dimensional (2D) nanosheets, and three-dimensional (3D) heterarchical structures. 1D nanofibers possess unique merits, such as high surface area, great surface-to-volume ratio, and excellent mechanical strengths and flexibility. Nanofiber electrodes can accommodate large volume variations and provide interconnect conductive paths during cycles. One of the most effective strategies for manufacturing nanofiber electrodes is electrospinning, which has been demonstrated in many applications [14]. Properties for electrospun nanofibers, such as the diameter, porosity, compositions and structure, are ready to be adjusted by tuning the electrospinning parameters. Therefore, hollow [15], core-shell [16] and hierarchical porous [17] nanofibers have been successfully prepared for different battery components. For lithium-ion batteries, electrospun polymer nanofibers are potential candidates for separators and polymer electrolytes [18, 19], and electrospun CNFs have been widely used as anode active materials, current collectors and conductive additives [20, 21]. Similar to that of the LIBs, the applications

of polymer nanofibers are focused on gel-electrolyte and separator, and CNFs mainly play the role to provide 3D conductive networks for post-Li ion batteries. CNFs as anode active materials is only for NIBs, KIBs. Electrospun polymer nanofibers and CNFs applied to LIBs has been researched for decades years. Nevertheless, for some post-Li ion batteries, especially the multivalent-ion batteries, the applications of the electrospun nanofibers are still in the initial stage.

Electrospun nanofibers can be converted into CNFs by carbonization. CNFs, CNTs and graphene all belong to carbon materials, which are widely exploited as conductive additives, electrode materials and substrates for supporting active components. In general, CNTs and graphene display better conductivity than CNFs, CNFs have their unique advantages, such as low cost, easy to fabricate, flexible creation of various architectures like hollow and hierarchical porous structure. Besides, owing to its large length to volume ratio, CNFs are facile to build 3D self-supporting network, resulting in a high energy density when used as hosts toward binder-free and flexible electrodes. Furthermore, the surface chemistry of electrospun CNFs can be easily adjusted by both synthesis (e.g., injection system, the constitution of polymer solution) and post-synthesis process conditions (e.g., heat treatment, activation process), which facilitates CNFs as functional components to satisfy different requirements [22, 23].

In this review, we mainly focus on surveying the recent advances of electrospun nanofibers for the emerging and growing post-Li ion battery technologies, such as Li-S, Na-ion, K-ion, multivalent ion batteries. Issues related to the advantages and challenges of electrospun nanofibers in new battery systems are also discussed. Finally, we examine the major issues facing electrospun nanofibers for practical post-Li ion battery applications with perspectives.

2. Electrospinning nanofibers

The concept of electrospinning can be traced back to the early 1930s when Formhals spun the cellulose acetate fibers in acetone [24, 25]. Although significant improvement has been made since then, the basic theory is the same that polymer solutions (or polymer melts) are converted by strong electrostatic force into continuous nanofibers with diameters of nanometers in size. Electrospinning technology is simple and easy to manipulate, which has been divided into melt electrospinning and solution electrospinning [24, 25]. Melt electrospinning using solvent-free polymer melts at elevated temperatures (*i.e.*, 200 °C) has been considered more desirable in tissue engineering, wound dressing and textile applications, which require large (>500 nm) and strong nanofibers without toxic solvent. In contrast, solution electrospinning using polymer solutions possesses merits in preparing nanofibers with small diameters, easy setup, and low energy consumptions. Solution electrospinning has been widely used in energy storage applications [23, 26].

Figure 1 shows a typical electrospinning apparatus, which consists of a grounded collector, a high voltage power source, and a spinneret [23-25]. When a high voltage is applied between the grounded collector and the spinneret, a strong electrostatic force is generated in between and forced on the charged polymer solution. When increasing the external voltage, the surface tension of the polymer solution is balanced by the electrostatic force to form a hemispherical contour, the so-called “Taylor cone”. Once the voltage is further improved, the balance on the Taylor cone is broken and a polymer jet will be ejected from the spinneret to the collector. During which process the solvent evaporates and the dry nanofibers are obtained [23-25]. The detailed mechanisms behind the electrospinning process are complex and still under debate. For example, the dynamics and chaos phenomenon during electrospinning were interpreted with different models [27].

Nonetheless, it is certain that continuous nanofibers are easy to be obtained via electrospinning owing to the electrostatic repulsive force driving the elongation of the viscous polymer solutions.

Electrospun nanofibers are versatile in chemical components, structure and morphology. Electrospun polymer nanofibers can be directly utilized as separators [28], or carbonized into carbon nanofibers (CNFs) to function as electrodes in rechargeable batteries [29, 30]. The nanofiber components can be tuned by changing the precursors, for example, Fe_3C/CNF has been prepared by electrospinning polyacrylonitrile (PAN) and iron (III) acetylacetonate mixtures [31]. Alloy/CNF electrodes have also been prepared by adding metal precursors in PAN solutions [32]. The morphology of electrospun nanofibers is affected by factors including the viscosity of polymer solution, electric field, feed rate, injection needle structure, and the heat-treatment conditions. Porous CNFs have been obtained by electrospinning PAN/poly (methyl methacrylate) (PMMA) blended polymer [33], where PMMA was a sacrificial component to create pores during heat-treatment. **Figure 1** shows different structures for electrospun nanofibers, such as core-shell, porous, tube-in-tube and tube-in-fiber, which can be obtained by adjusting the needle nozzle configuration and polymer precursors during electrospinning [23, 34]. The above parameters can be accumulated to design specific nanofiber structures based on different end applications.

It is worth noting that electrospun nanofibers are usually carbonized into CNFs as conductive additives/scaffolds for energy storage applications [34]. The neat nanofibers need to be stabilized in the air at 200-300 ℃ before carbonization at 500-1000 ℃ in an inert atmosphere. Because direct carbonization of neat fibers at high temperature induces fusing reaction, the pre-treatment of stabilization in the air could transform the thermoplastic neat fibers into highly coagulated thermoset fibers, thereby preventing the fiber from fusing during the following carbonization process [35]. The graphitization degree of CNFs is positively related to their electric

conductivity. For example, the electrical conductivity for CNF has been increased from 0.05 S cm^{-1} to 1.22 S cm^{-1} by increasing the carbonization temperature from 800 ℃ 1000 ℃ [36]. However, high-temperature annealing is energy-consuming and unfavorable to maintain small active particles inside CNFs, if any.

3. Applications of electrospun nanofibers in post-Li ion batteries

3.1 Lithium-sulfur battery

Rechargeable Li-S batteries (LSBs) have attracted intensive interests from both the research and industry communities due to their high theoretical energy density and the low cost of sulfur feedstock. Although the sulfur cathodes possess a high theoretical capacity of 1673 mAh g^{-1} with reversible reactions between sulfur and Li_2S (**Figure 2**a, b), the practical capacity is usually low with rapid capacity decay [9, 10]. The low utilization of activity materials is attributed to the electrically and ionically insulating sulfur and lithium sulfides. In addition, during charge and discharge, the reaction intermediates, long-chain lithium polysulfides (LPSs), are ready to dissolve in electrolytes and diffuse to the lithium anode, leading to high irreversible capacities. In the Li metal anode side, unstable solid electrolyte interphase and dendrite formation cause serious safety issues. Over the past decades, remarkable progress has been achieved in improving LSBs performance [9]. In this section, we will aim at surveying the contributions of electrospinning technology regarding CNF/sulfur cathodes, CNF interlayers and hybrid nanofibers for high performance LSBs.

3.1.1 Electrospun nanofibers for sulfur cathodes

Porous CNFs with high electric conductivity and large pore volume are ideal hosts for insulating sulfur particles as advanced cathodes for LSBs [37-39]. The functional groups on the surface of electrospun CNFs are beneficial to immobilize polysulfides with strong chemical interactions, thus

increasing the cyclic capacities for LSBs [40-42]. Therefore, CNFs with copious morphological and chemical structures have been intensively investigated for sulfur cathodes.

In an early study, Zhang *et al.* [33] used PMMA as a sacrificial polymer to prepare porous CNFs as sulfur hosts in **Figure 2**c. During carbonization at 1000°C, PMMA was removed to form nanopores, where sulfur particles were impregnated later via chemical solution reactions. It was observed that the conductivity of PCNFs decreased from 1.8 S cm^{-1} to 0.52 S cm^{-1} after sulfur impregnation, which value is still magnitudes higher than the 5 $\times 10^{-30}$ S cm^{-1} for sulfur [9]. Thus, high discharge capacity of 1400 mAh g^{-1} at 0.05 C and rate capacity of 900 mAh g^{-1} at 0.2 C were obtained for the PCNF/S-42 (with 42 wt% of sulfur content) as shown in **Figure 2**c, indicating improved sulfur utilization. However, a high capacity fade rate of 0.5% was observed for the PCNF/S-42 cathode after 30 cycles due to the poor affinity of nanopores to LPSs. In fact, there is a tradeoff between the pore size and the S/PCNF cathode performance. CNFs with micropores ($\leq$ 2nm) can alleviate the polysulfides diffusion by strong capillary force or physical confinement to improve cyclic stability. However, the sulfur loadings were limited to be below 40wt.% for microporous CNF/S cathode due to the low pore volumes [43]. Meso and macroporous CNFs can provide large spaces for high sulfur contents, but polysulfides are ready to dissolve in the electrolyte, resulting in short cycle life [43, 44]. Thus, a balance must be struck between the sulfur loading and the cycle life for porous CNF/S cathodes.

An effective strategy to obtain both high capacity and high sulfur content is to prepare hollow porous CNFs hosts. Manthiram *et al.* [44] designed sulfur-embedded activated multichannel carbon nanofibers (S-a-MCNF) through a facile single-nozzle co-electrospinning technique. During electrospinning and carbonization, PAN formed the outer layer carbon wall while the inner PMMA was decomposed into hollow channels to accommodate sulfur particles.

Micropores were further created on the carbon walls by KOH activation to facilitate charge transfer and block LPSs outward diffusion. The S-a-MCNF cathode with a high sulfur content of 80 wt% presented an initial capacity of 1351 mAh g^{-1} and maintained 920 mAh g^{-1} after 300 cycles at 0.2 C. Under a high sulfur loading of 4.6 mg cm^{-2}, the S-a-MCNF cathode also exhibited an excellent reversible capacity of 753 mAh g^{-1} after 200 cycles, indicating high cyclic capacities for hollow PCNF/S structures. Another strategy is to properly design meso and micropores on CNFs, which operates synergistically to enlarge sulfur loading and suppress the polysulfide diffusion. One representative example is reported by Gong *et al.* [17] who prepared a hierarchical porous carbon fiber (HPCF) with a few mesopores by using SiO_2 template and abundant micropores by KOH activation, respectively. The meso and micropore size distributions were adjusted by changing the contents of SiO_2 and KOH, respectively. Consequently, the optimal HPCF/S cathodes deliveredhigh capacity retention of 88.4% after 100 cycles at a high sulfur content of 66 wt.%. With similar strategies, other porous or/and hollow CNF/S cathodes have also been successfully synthesized for high loading and high capacity LSBs[30, 38, 40].

The electrical conductivity of electrospun CNFs is another crucial parameter for CNFs/S cathodes, especially at high rates. As mentioned in Section 2, polymer (*i.e.*, PAN)-derived CNF with amorphous structure usually present low electrical conductivities and poor graphitization degrees [34, 45], especially compared to chemical vapor deposited carbon nanotubes (CNTs). To improve the conductivity of electrospun CNFs, several approaches have been developed. The first is to introduce transition metal nanocrystals (*i.e.*, Mn, Co, Ni) to catalyze the formation of graphitic carbon layers at moderate temperatures (*i.e.*, 650 ℃) [31, 46, 47]. The metal nanocrystals in CNFs would be removed by acid etching to create nanopores, which serve as sulfur containers. For example, Xu *et al.* [29] prepared PCNFs by mixing iron (III) acethylacetonate and PAN as polymer

solutions for electrospinning (**Figure 3**a). During carbonization at 750 °C, the iron (III) acethylacetonate was converted to Fe_3C nanoparticles (10-75 nm) surrounded by graphitic carbon layers, forming Fe_3C/CNF. After acid etching, PCNFs with graphitic carbon layers were received, presenting a much higher electrical conductivity of 10^{-2} S cm^{-1} than the 10^{-5} S cm^{-1} for the bare CNFs. As a result, the rate capacities of LSBs with graphitic PCNF/S were significantly higher than those with amorphous PCNF/S, arriving 906, 799, 742 and 697 mAh g^{-1} at 0.3 C, 1 C, 1.5 C and 2 C, respectively (**Figure 3**b). Similarly, Co-decorated CNF/S [48] and FeO catalyzed graphitic PCNF/S cathodes [49] have also been prepared to show high rate capacities (*i.e.*, ~800 mAh g^{-1} at 1C for Co-decorated CNF/S and 670 mAh g^{-1} at 2C for graphitic PCNF/S) [50]. This clear trend delivers a message that high graphitization of electrospun CNF is essential for PCNF/S cathodes to obtain high sulfur utilization and high-rate capacities in LSBs.

Another effective method to improve the conductivity of electrospun CNF is to add highly conductive sp^2 carbon materials like CNT (10^2-10^6 S cm^{-1}) and graphene (10^6 S cm^{-1}) [15, 51]. Chen *et al.* [15] built a porous hollow CNTs/CNFs-S composite (**Figure 3**c) by electrospinning PAN, PMMA and nickel acetate ($Ni(Ac)_2$) mixture into nanofibers and annealing in the reductive atmosphere. The PAN was carbonized into CNF and PMMA was catalyzed by Ni to CNTs. The conductivity of the electrospun nanofibers was enhanced by introducing CNTs. Consequently, excellent rate capability for the CNTs/CNFs-S composite cathodes was achieved with high capacities of 1313, 1078, 878 and 803 mAh g^{-1} at 0.2 C, 0.5 C, 1 C and 5 C, respectively (**Figure 3**d). Even at 1C and 5C, the reversible capacity remained 700 and 430 mAh g^{-1} after 200 circles (**Figure 3**e). Another method to introduce CNTs is to directly electrospun the commercial CNT with PAN polymer, followed by carbonization [52]. The CNF-CNT/S composite cathode delivered enhanced electrochemical performance with a reversible capacity of 637 mAh g^{-1} at 50 mA g^{-1}

after 100 cycles and 437 mAh g^{-1} at a high current density of 1 A g^{-1}, which values were superior to the CNF/S counterpart. Other CNTs modified CNFS/S cathodes have also been reported [53-55]; without surprise, the introduction of CNTs significantly enhanced the reaction kinetics and high-rate capacities for S/CNF/CNT cathodes. Reduced graphene oxide (rGO) or/and graphene sheets have also been incorporated into CNFs either before or after electrospinning [56, 57]. Chu *et al.* [56] synthesized rGO coated porous CNF/S flexible paper (rGO/S-PCNP) as a cathode by surface coating electrospun S-PCNP with rGO, which not only improved the conductivity of the composite electrode but also entrapped LPSs by strong chemical absorption during cycles. The rGO/S-PCNP cathodes with a sulfur content of 58.4 wt% exhibited a high discharge capacity of 623.7 mAh g^{-1} at 0.1C after 100 cycles. Rate capacity was maintained at 690 mAh g^{-1} at 0.5C. Han *et al.* [57] directly electrospun rGO to CNFs. Benefiting from the highly conductive 3D network, CNF/rGO/Li_2S_6 cathodes demonstrated a high areal capacity of 15.5 mAh cm^{-2} under an extremely high sulfur loading of 20.3 mg cm^{-2}.

Physical confinement of polysulfides by nanopores cannot completely inhibit their diffusion for long term cycles due to the relatively week interactions between the nonpolar carbon and the polar polysulfides. To overcome this obstacle, strong chemical interactions between polysulfides and polar surfaces or particles on CNFs have been exploited. The surface chemistry of CNFs was engineered by oxygenated functional groups, heteroatom doping and polymer/metal oxide coating. Liang *et al.* [58] selected PVP and polyvinyl alcohol (PVA) as carbon sources to fabricate porous CNFs using electrospinning. The cathode with N-doped porous CNFs derived from PVP exhibited a much lower capacity decay rate of 0.027% per cycle than the 0.127% for PVA-derived porous CNF/S cathode without N-doping (**Figure 4**a). The dissimilarity demonstrated the benefit of N doping on LPS anchoring in S/PCNF cathodes. Wang *et al.* [42]

decorated CeO_2 nanocrystals on 3D porous N-rich carbon nanofiber (CeO_2/CNF). Compared with the cathodes without CeO_2, the S/CeO_2/CNF displayed a higher initial capacity of ~1220 mAh g^{-1} and a lower capacity decay rate of 0.015% per cycle over 400 cycles at 0.2 C. More importantly, the S/CeO_2/CNF delivered a competitive areal capacity of 6.7 mAh cm^{-2} after 30 cycles under a high sulfur loading of 8.6 mg cm^{-2}, indicating the effectiveness of polar catalysts in optimizing LSB performance.

Besides pure CNFs, hybrid nanofibers, such as metal oxide/(CNF) nanofibers and polymer nanofibers, have also been synthesized by electrospinning for LSBs. Ma *et al.* [59] prepared TiO_2 nanofibers using electrospinning poly (vinylpyrrolidone) and tetrabutyl titanate in ethanol followed by annealing in the atmosphere. Recently, our group integrated black phosphorus quantum dots (BPQDs) into electrospun PCNFs/S as sulfur cathodes [46]. Both experimental and theoretical calculations results revealed that BPQD could effectively anchor and catalyze the reduction of polysulfides. The exceptional activity was attributed to the numerous electrocatalytically active edge sites of BPQDs. *In-situ* transmission electron microscopy (TEM) observations indicated a large volume expansion of PCNF/S/BPQD cathode during lithiation (**Figure 5**a-c), whereas, in-situ transparent battery presented no color change of electrolyte in PCNF/S/BPQD battery, suggesting effective immobilization of polysulfides by BPQD cathodes. As a result, the PCNFs/S/BPQD cathode showed an initial capacity of 1234 mAh g^{-1} at 0.1C (capacity remained 1072 mAh g^{-1} after 200 circles), and reversible rate capacities of 910, 821 and 784 mAh g^{-1} at 1, 2 and 4 C ((**Figure 5**d, e). In addition, the cathode exhibited exceptional cyclic stability with a capacity fading rate of 0.027% per cycle over 1000 cycles and remarkable capacity retentions of over 90% at high sulfur loadings up to 8 mg cm^{-2}.

Electrospun polymer nanofibers have also been utilized in sulfur cathodes. Ye *et al.* [60] designed sulfur/carbon (S/C) nanocomposite-filled PAN nanofibers (denoted as S/C/PAN) for long life and high capacity LSB cathodes. Similarly, Sandugash *et al*. [61] prepared PAN nanofibers filled with S/KB (Ketjen Black, conducting matrix) particles as cathode. The Nafion nanoweb has also been deposited onto the sulfur cathode by electrospinning [62] for nanoweb structure owning higher electrolyte wettability, which formed fast ion migration channels and thus facilitated the redox reactions in LSBs [63].

3.1.2 Electrospun nanofiber as interlayer and separator

In 2012, Manthiram's group proposed to use microporous carbon paper as an interlayer between cathode and separator to block the diffusion of polysulfides to Li metal anode in LSBs [64]. This novel configuration was designed bifunctional to reduce the LPSs diffusion and to reuse the captured LPSs as shown in **Figure 4**b. The concept of interlayer has attracted a lot of attention, among which electrospun CNFs played essential roles. Manthiram's group [65] explored the effects of thickness, surface area, and pore size distribution of CNFs interlayer on the electrochemical performance of LSBs. Various CNF interlayers, including nonporous carbon nanofibers (NPCNFs), microporous carbon nanofibers (ACNFs) and meso-micro-pores carbon nanofibers (MCNFs) were prepared by electrospinning and activation. It was found that after 100 cycles at 0.2C, cathodes with MCNFs interlayer with the largest surface area claimed the highest capacity retention (capacity retention of NPCNF, ACNF, MCNF:73.91%, 79.98%, 83.06%). With increasing the thickness of the CNF interlayer, the cyclic capacity retentions were also improved. It is clear that thick PCNF interlayers with large surface areas are more favorable to obtain stable LSBs. Huang *et al.* [31] electrospun iron (III) acetylacetonate (precursor for Fe_3C) and PAN to

produce Fe_3C/CNFs interlayers. Fe worked as a catalyst to improve the graphitization of PAN at a low temperature (650 ℃), which was important to keep N-containing functional groups on the CNFs. The Fe_3C/CNF interlayers with improved conductivity effectively suppressed the dissolution of polysulfides and improved the utilization of active particles. A high discharge capacity of 893 mAh g^{-1} was shown after 100 cycles, rendering capacity retention of 76%.

Metal oxides (*i.e.*, TiO_2 [66], MnO_2 [67], and MgO [68]) possessing strong chemisorption capability to polysulfides have also been incorporated into electrospun CNFs as functional interlayers in LSBs. Liang *et al.* [41] introduced TiO_2 nanoparticles into CNFs (designated as CNF-T interlayer) by a "dip and dry" method. The stacked conductive CNF network provided fast-electronic paths and large space to relieve the volume changes of active materials during cycling. The CNF-T interlayer inserted LSBs presented excellent electrochemical performance with an initial reversible capacity of 935 mAh g^{-1} at 1 C and remarkable capacity retention of 74.2% after 500 cycles (**Figure 4**c). To ameliorate the battery performance under high sulfur loadings, Zhuang *et al.* [69] prepared MoO_2-CNFs interlayers by electrospinning PAN and phosphomolybdic acid (PMA: H_3PO_4•$12MoO_3$) mixture, followed by carbonization. The battery with MoO_2-CNFs interlayers showed a high areal capacity of 5.11 mAh cm^{-2} and an excellent rate capacity of 865 mAh g^{-1} at 8.4 mA cm^{-2} under a sulfur loading of 2.5 mg cm^{-2}.

So far, it is clear that electrospun nanofiber interlayers can effectively block the diffusion of polysulfides and effectively elevate the cyclic and rate capacities of LSBs, even under high sulfur loading conditions. Nevertheless, it is worth noting that interlayers are electrochemically inert in LSBs, thus heavy CNF/metal oxides interlayers would decrease the overall sulfur content in cell level, leading to practically low energy densities. To be worse, thick interlayers require excess amounts of electrolyte to wet the electrodes and interlayer, further lowering the practical

energy densities based on the total mass of LSBs. It is suggested to take these two issues into account in future research for interlayers.

Separator and electrolyte in LSBs have also been prepared by electrospinning. Rao *et al.* [70] immersed electrospun PAN/PMMA membrane into LiTFSI in $PPR_{14}TFSI$ or LiTFSI in $PPR_{14}TFSI$ + PEGDME to produce gel polymer electrolytes (GPE). Separators for LSBs are expected to possess great ionic conductivity, high thermal stability, and the capability to prohibit "shuttle effect". The conventional polypropylene (PP) membrane separators, however, present low porosity, poor electrolyte wettability and poor LPSs affinity [71, 72]. To this end, PAN and ammonium polyphosphate (APP) were electrospun into a PAN@APP nonflammable multifunctional separator by Lei *et al.* [28]. For the PAN@APP separator, APP had abundant amine groups and phosphate radical, which suppressed the LPSs diffusion via Lewis acid-based bonding. The refractory APP increased the stability of battery performance at high temperatures (**Figure 6**a). The capacity retention of 83% over 800 cycles was demonstrated for LSBs using PAN@APP separators. Even at 75℃, the capacity retention was 78% after 100 cycles (**Figure 6**b). Zhou *et al.* [73] fabricated a double-layered MOF-PAN/rGO-PAN nanofiber membrane as an advanced separator for LSBs in **Figure 6**c. MOF particles and rGO sheets having strong absorption to LPSs work as ion-selective membranes, which provided a fast path to Li-ions and blocked the LPSs shuttling. LSBs with MOF-PAN/rGO-PAN nanofiber separator displayed a high initial capacity of 1302 mAh g^{-1} at 0.5C (**Figure 6**d) and low-capacity loss per cycle 0.03% per cycle over 600 cycles at 5C.

The above discussions clearly demonstrate the effectiveness of electrospun nanofibers in ameliorating the electrochemical performance for LSBs (**Table 2**). The battery performance is closely related to the properties of electrospun nanofibers, in terms of conductivity, porosity and

surface chemistry, which warrants further discussions. (1) The high electrical conductivity of CNFs is of great importance to offer a fast charge transfer and improved redox reaction kinetics. The electrical conductivity of CNFs can be improved by introducing transition metal salts or transition metal (Mn, Co, Ni) as catalysts to improve graphitization degrees of CNFs. Also, highly conductive CNT and graphene can be added to improve the electrical conductivity. (2) The micropores and mesopores can alleviate the LSPs diffusion by physical confinement. However, micropores or mesopores alone cannot balance the electrode stability and sulfur loading for LSBs, thus, hierarchical structure [17], porous hollow structure[15] have been reported to combine the advantages for macropores, micropores and mesopores for high-loading, high capacity and high power sulfur cathodes as listed in **Table 2**. (3) Oxygenated functional groups, heteroatom doping and polymer/metal oxides can enhance the electrochemistry performance of LSBs through strong chemical interactions and catalytic effects with LPSs [50]. Compositing functional groups or catalysts with porous CNFs is suggested to be a promising method further to improve the electrochemical performance for long-term cycling LSBs. (4) Electrospun CNFs can build flexible cathodes, interlayers, and separators owing to their excellent mechanical property. For example, the rGO/S-PCNP paper [56] and NPCFs/S [51]) as self-supporting cathodes, can be bent without damage.

Notably, electrospinning has also been utilized to produce as Li metal scaffold, the separator and polymer membrane for polymer gel electrolyte to protect lithium metal anodes [74-76].

3.2 Sodium-ion battery

Compared to the limited lithium, sodium is ubiquitously and inexhaustibly dispersed in the Earth crust like seawater. SIBs with potentially lower cost and larger availability have been considered

more appealing than LIBs to serve large-scale energy storage applications. As mentioned in the Introduction, SIBs possess a similar working principle to that of LIBs, where Na ions are shuttling between the anodes and cathodes during charge/discharge (**Figure 7**a). However, Na^+ has a larger molar mass and ionic radius than Li^+ (**Table 1**), leading to lower energy densities for SIBs [77]. In addition, the larger Na ions also induce large volume expansions during sodiation of electrode materials, especially for alloys and metal oxides. Electrospinning has been confirmed an effective technique to prepare high performance CNF composite electrodes in SIBs, such as CNF anode, metals and alloys, metal oxides (*e.g*. SnO_2, Fe_2O_3, Sb_2O_3 and TiO_2)/CNF anodes [32, 78, 79], transition metal dichalcogenide (*e.g*. SnS_2, MoS_2, FeS_2, $FeSe_2$ and $MoSe_2$)/CNF anodes [80-82] as well as CNF-modified cathodes [83].

3.2.1 Electrospun nanofibers for anode

Although graphite is known to be the most successful anode in commercial LIBs, their application in SIB anode is not trivial because Na ion direct intercalation in graphite is thermodynamically unfavorable in carbonate electrolyte[84]. We found that Na ions can be reversibly intercalated in graphite through co-intercalation reactions in ether-based electrolytes [85]; however, the Na storage capacity is close to 100 mAh g^{-1}, which is much lower than the 372 mAh g^{-1} for graphite anode in LIBs. Instead, non-graphite carbon materials are shown to present important capacities of 200-300 mAh g^{-1} and long cycle life. Electrospun CNFs have been intensively investigated as anodes in SIBs.

Zhang *et al.* [86] fabricated CNFs by annealing electrospun PAN fibers at 650 ℃ to 2800℃ to explore the relationship between microstructure and Na storage behavior in hard carbon. They found that low temperature (650-950 °C) made CNF contain copious amounts of O and N heteroatoms, high disorder structure and high amounts of micropores, which induced great Na

storage capacities of over 300 mAh g^{-1} and apparent discharge/charge slops (**Figure 7**b,c). When increasing the carbonization temperature to above 1000 °C, the electrochemically active heteroatoms and micropores were removed, the reversible capacity decreased accordingly. At temperature above 2000 °C, the CNFs showed a high graphitization degree in TEM images, and a single voltage plateau of about 0.1 V was observed which was attributed to the Na insertion reaction in graphite. The reversible capacity was further decreased to 200 mAh g^{-1} for CNF carbonized at 2500 °C (**Figure 7**c). It is noted that the Na storage mechanisms in hard carbon materials like CNFs are still under debate [87, 88], which needs intensive experimental and theoretical studies in the future.

Nanopores and functional groups in electrospun CNFs can function as additional active sites to Na ion storage in SIBs, thus various porous CNFs have been prepared for high capacity anodes. Han *et al.* [30] prepared hollow carbon nanofibers (HCNFs) using in situ polymerizing PANI on electrospun PMMA nanofibers, then removing PMMA and heat-treating the PANI fibers. The 1D hollow structure shortens the electron/ion diffusion paths and presents great mechanical stability, which is beneficial to high-rate performance in SIBs. The HCNFs exhibited a high charge capacity of 326 mAh g^{-1} at 20 mA g^{-1} and great capacity retention of 70% after 5000 cycles at a high current rate of 1.6 A g^{-1}. To further promote the Na ion transfer in CNF and enlarge the contact area between the electrode and electrolyte, Shan *et al.* [89] reported freestanding N-doped hierarchically porous carbon pellicles (CZIF-8/PAN) as SIB anodes (**Figure 8**a). The hierarchical pores were produced by introducing the ZIF-8 template, which largely increased the surface area and pore volume of CNFs. In addition, N-doping in CZIF-8/PAN improved the electrical conductivity and the number of Na ion storage sites. As a result, the CZIF-8/PAN carbon pellicles showed an initial discharge/charging capacities of 374.3/285.3 mAh g^{-1} at 0.05 A g^{-1} (**Figure 8**b),

and a high reversible capacity of 186.2 mAh g^{-1} as well as excellent cyclic stability of 93.5% retention after 600 cycles at 1.0 A g^{-1}. At an extremely high current density of 5 A g^{-1}, the CZIF-8/PAN anode exhibited a reversible capacity of 153 mAh g^{-1}, which is higher than the ≈70 mAh g^{-1} for CZIF-8 after 150 cycles and ≈120 mAh g^{-1} for CPAN after 600 cycles, indicating the importance of nanopores for high-rate anodes in SIBs.

Transition metal sulfides are high capacity anodes for SIBs, however, the low electronic conductivity, unstable structure, and large volume variation during cycling impeded their practical applications. Fortunately, the carbon matrix as excellent hosts can provide enough space for volume expansion, high conductivity for electron/ion transportation, robust structure to prevent aggregation [81, 90]. For example, *Liu et al.* [81] prepared a flexible MoS_2@CNFs anode, where 2H-MoS_2 nanosheets were uniformly grown on CNFs by L-cysteine-assisted hydrothermal method, as shown in **Figure 8**c. A high specific capacity (528 mAh g^{-1} at 100 mA g^{-1}), rate performance (412 mAh g^{-1} at 1 A g^{-1}), and long cycle life (over 600 cycles at 1 A g^{-1}) were obtained using MoS_2@CNFs anodes (**Figure 8**d). The attractive battery performance was attributed to the excellent electrical conductivity of the 3D carbon matrix and the strong C-O-Mo chemical bonding. Further, Liu *et al.* [82] designed a 3D carbon matrix of CNFs interpenetrating graphene sheets (CNFIG) for MoS_2. 4,4′-oxidianiline and pyromellitic dianhydride were dissolved in dimethylacetamide (DMAc) as the electrospinning solution. MoS_2 was introduced into CNFIG through hydrothermal reaction. The short CNFs vertically located on graphene sheets prevented the graphene from restacking, indicating exceptionally high mechanical integrity and electrical conductivity. The MoS_2 was homogeneously deposited on the CNFIG framework, making them completely expose to the electrolyte, thus leading to a high specific capacity of 598 mAh g^{-1}, long-term cycling stability up to 1000 cycles, and an excellent rate performance (up to 10 A g^{-1}). Similar

structures, such as Fe_7Se_8/N-CNFs [80], have also been successfully prepared for high capacity SIB anodes.

Metal (oxides) are another category of anodes for SIBs with suitable redox potential and high capacities [91, 92]. Similar to transition metal sulfide compounds, electrospun CNFs cooperated with metal oxide materials can mitigate the challenges of low electric conductivity and large volume changes during sodiation/desodiation. Wang *et al.* [91] reported TiO_2/C nanofibers produced by electrospinning, annealing, and plasma treating. The plasma technique introduced edge-dangling bonds, defects, and oxygen-containing functional groups to TiO_2/C, which improved the ionic conductivity and active surface areas. After 500 cycles at a high current density of 10 C, the battery maintained a high capacity of 191 mAh g^{-1}. CNF hosts are beneficial to limit the growth of the metal oxide particles during heat treatment, which is important to obtain a high rate and long cycle anodes in SIBs. Xu *et al.* [32] reported atomic scale, amorphous FeO_x/CNF films by electrospinning. They claimed that the formation of ultrafine FeO_x particles was possible because of the optimal carbonization temperature and duration as well as the strong constraint provided by the surrounding CNF matrix, resulting in a lack of energy required for growth of large FeO_x crystals. The FeO_x/CNF composites in SIBs delivered a capacity of 277 mAh g^{-1} at 0.5 A g^{-1} with maintaining 100% capacity after 500 cycles and a rate capacity of 169 and 124 mAh g^{-1} at 4 and 8 A g^{-1} (**Figure 8**e, f). The exceptionally high cyclic stability was attributed to the unique structure that full encapsulation and uniform dispersion of FeO_x in the CNF matrix prevented aggregation and large volume expansion of active particles. Note that remarkable cyclic stability and excellent capacity for FeO_x/CNF were also presented in LIBs.

3.2.2 Electrospun nanofibers for cathode

Transition metal oxide compounds, polyanionic compounds, Prussian blue analogs and organic materials have been widely investigated as advanced cathode materials in SIBs [5]. Na_xMO_2 compounds (M = Fe, Mn, Ni, Co, Cr, Ti, V) are appealing transition metal oxide cathode materials for SIBs by virtue of high theoretical capacities and facile 2D Na ion diffusion channels. However, Na_xMO_2 suffers poor cyclic stability due to the volume change during Na ion extraction/insertion. Electrospun 1D nanostructure can stabilize Na_xMO_2 for long-cycle SIB cathodes [93, 94]. Liu *et al*. [94] electrospun porous P2-$Na_{2/3}Ni_{1/3}Mn_{2/3}O_2$ nanofibers using PVP sacrificial phase and $Mn(CH_3COO)_2{\cdot}4H_2O$, $NaNO_3$, Ni $(NO_3)_2{\cdot}6H_2O$ metal precursors. During the annealing process, PVP was fully decomposed gases (such as CO_2 and H_2O) to create pores within nanofibers assembled by active nanoparticles (**Figure 9**a). The porous nanostructure provided individual particles easy access to electrolyte, fast electron/Na^+ transport kinetics and robust structures during cycling. Exceptionally high rate capability (166.7 mAh g^{-1} at 0.1 C with 73.4 mAh g^{-1} at 20 C) as shown in **Figure 9**b and durable cycling life (80.8% capacity retention after 500 cycles) were achieved for the fibrous cathode. The P2-$Na_{2/3}Ni_{1/3}Mn_{2/3}O_2$ cathode has also been paired with a hard carbon anode into a Na ion full cell, which presented a distinguished energy density of 212.5 Wh kg^{-1} (**Figure 9**c).

Ultralong $NaCrO_2$ nanowires (NWs) as wide-temperature-operating cathodes for SIBs have also been constructed [95]. The olive-green $NaCrO_2$ NWs were prepared by electrospinning and two-step heat treatments. The 1D NWs with diameters of about 48 nm and lengths of 30 μm composed of ultrafine $NaCrO_2$ nanocrystals (3-5 nm). The amplified electrode/electrolyte surface area gave rise to fast electronic/ionic transfer and high electrochemical utilization. The $NaCrO_2$ NWs cathode presented excellent high-rate capacities at 10 C for 300 cycles under a wide range of temperatures, *i.e*., 60.1 mAh g^{-1} at -15 °C with 80.6% capacity retention, 108.8 mAh g^{-1} at

25 °C with 88.4% capacity retention, and 94.6 mAh g^{-1} at 55 °C with 86.9% capacity retention. Encouragingly, $NaCrO_2$ NWs//hard carbon full cell also showed a competitive energy density of 161 Wh kg^{-1}, suggesting their potential applications in a practical environment.

Polyanionic compounds (such as $NaVPO_4F$, $NaFePO_4$) have attractive properties of stable crystal structures and high working potentials, but the low electronic conductivities limit the reaction kinetics. Electrospun carbon nanofibers can work as conductive frameworks for polyanionic compounds for high power SIB cathodes [83]. Jin *et al.* [96] synthesized self-standing $NaVPO_4F$/C nanofibers through electrospinning and heat treatment. PVP was the carbon source to generate carbon matrix by annealing, during which CO_2 was released to create pores (**Figure 9**d). This structure presents many advantages, namely: the shorten Na ion transportation pathway for ultrasmall $NaVPO_4F$ nanoparticles (~6 nm), the facilitated penetration of electrolytes through porous structure, and the vigorous structure of the 3D $NaVPO_4F$/C networks. As a result, high capacity (126.3 mAh g^{-1} at 1 C) and long cycle life (96.5% capacity retention after 1000 cycles at 2 C) were displayed. More importantly, the highly conductive CNF host endowed $NaVPO_4F$/C with an exceptionally high-rate capability of 61.2 mAh g^{-1} at 50 C. Further, the $NaTi_2(PO_4)_3$//$NaVPO_4F$/C full cell displayed an initial discharge capacity of about 80 mAh g^{-1} and maintained 65.7 mAh g^{-1} after 50 cycles (**Figure 9**e). An important message from this work is that decreased particle size and uniform carbon coating are highly anticipated to realize high power and long life polyanion cathodes. Following this strategy, Na_2FePO_4F/C cathode with ultrafine Na_2FePO_4F nanoparticles (~3.8 nm) has also been prepared by electrospinning [97]. Electrochemical characterizations revealed that the Na_2FePO_4F/C presented an impressive high-rate capacity of 46.4 mAh g^{-1} at 20 C and exceptionally high capacity retention of 85% after 2000 cycles. It is noted that the electrospun neat fiber-Al sample was directly annealed into binder-free

composite electrodes, where the "all-in-one" structure enhanced the electrochemical activity and reaction kinetics, as evidenced by the high Na diffusion coefficient of 2.07 $\times 10^{-13}$ cm^2 s^{-1}. To estimate the application of Na_2FePO_4F/C in practical SIBs, they further prepared Na_2FePO_4F/C //CNF full cells. The full cell exhibited an energy density of 135.8 Wh kg^{-1} and capacity retention of 84.5% after 200 cycles. Similarly, $Na_3V_2(PO_4)_3$/C core-shell NWs [98], $Na_3V_2(PO_4)_3$/C nanofiber [99], Na_2MnPO_4F/C nanofibers [100] cathodes have also been successfully demonstrated with significantly improved cyclic and rate performance in SIBs.

Organic materials with the environmentally benign property have also been investigated as SIB cathodes. For example, Cai *et al.* [101] prepared a poly (2-cyanoindole) nanofiber cathode to be assembled with Na metal anode and $NaPF_6$-based electrolyte into SIBs. The secondary battery presented a high output voltage of 3.2 V and reversible capacities of ≈100 mAh g^{-1} in the first 10 cycles. The rate performance of poly (2-cyanoindole) nanofiber cathode was moderate with capacities of 106 mAh g^{-1} at 0.2 C and 75 mAh g^{-1} at 10 C, rendering capacity retention of 71%, which is comparable to its LIB counterpart. Apparently, research on electrospun organic cathodes for SIBs is at its infant stage, and more efforts are suggested in the future.

In summary, electrospun nanofibers have played essential roles in providing advanced electrode materials for SIBs, such as CNF, transition metal sulfide or oxide/CNF anodes, and transition metal oxide or polyanionic nanofiber cathodes. Their material structures, synthesize methods and the electrochemical performance are summarized in **Table 2**. Electrospun CNFs can directly store Na ions as anode materials, whose performance is closely related to the intrinsic properties of hard carbon. Most CNFs served as a template or/and host to active particles for SIB electrodes, such as alloy/CNF anode and polyanionic compound/CNF cathode, whose performance is not only determined by the conductivity, porosity and mechanical stability for

CNFs also the property of active particles. To this end, more attention needs to be paid on the temperature-depend graphitization degree of CNF and the particle size of active particles. At low annealing temperatures, ultrafine and uniformly distributed active particles can be obtained, e.g., atomic-scale FeO_x/CNF [32], but the conductivity of CNF was low arising from the low graphitization degree of CNF host at low temperature. At high temperatures, the conductivity of CNF would be increased, whereas the accompanying large active particles are detrimental to stable cycling. Thus, the annealing temperature needs optimization for CNF/metal oxide electrodes in SIBs. Another aspect that requires attention is the content of CNF in CNF/metal oxide electrodes. CNFs serve as scaffold or host to active particles in CNF/metal oxide electrodes; if the CNFs content is too high, the specific capacities for CNF/metal oxide would be compressed, whereas too little CNF may induce instability of electrodes during cycling. Moreover, self-supporting flexible electrodes can be constructed by CNFs due to high mechanical strength, such as MoS_2@CNFs anode [81], FeO_x/CNF films anode [32] and $NaVPO_4F$/C nanofibers cathode[96]. These flexible electrodes are key components to develop flexible NIBs.

Besides electrode materials, electrospinning has also been utilized in preparing advanced separators (*i.e.*, poly(vinylidene fluoride) fluoride film [102]) and polymer electrolyte (*i.e.*, PVDF-based gel polymer electrolyte [103]) for high-performance SIBs.

3.3 Potassium-ion batteries

Similar to SIBs, KIBs have also been expected as low-cost candidates to replace the LIBs in large-scale applications. Different from SIBs, K^+/K possesses a reduction potential of -2.93V vs. SHE; it is 200 mV lower than the Na counterpart (-2.71V), thus potentially enabling higher voltage and energy density. In addition, the weaker Lewis acidity of K^+ than Na^+ ensures its higher mobility in electrolyte and at the electrode/electrolyte interface, implying faster kinetics for KIBs. Recently,

an astonishing amount of publications have been published about KIBs, associated with the efforts to improve the electrochemical performance of electrodes [104, 105]. Herein, we will focus on summarizing the state-of-the-art electrospun nanofibers as advanced anode and cathode materials for high-performance KIBs.

3.3.1 Electrospun nanofibers for anode

Electrospun CNFs have been directly utilized as anodes in KIBs, which presented an exceptionally long cycle life of 1200 cycles with a very low decay rate of 0.01% per cycle [106]. To further improve the K storage capacities in CNFs, Yang *et al.* [107] prepared a free-standing N-doped necklace-like hollow carbon (NHC). The NHCs were synthesized by electrospinning ZnO nanospheres/PAN/DMF solution, where ZnO functioned as a hard template to create pores (**Figure 10**a). The composites presented hierarchical pores with a high specific surface of 355.6 m^2 g^{-1}, which promoted the contact between the electrolyte and the active materials, thereby improving the reaction kinetics. The ultra-high N-doping led to higher electronic conductivity and stronger adsorption to K ions. The freestanding film showed a high reversible capacity of 293.5 mAh g^{-1} at 100 mA g^{-1}, outstanding rate property of 204.8 mAh g^{-1} at 2000 mA g^{-1}, and cycling performance of 161.3 mAh g^{-1} at 1000 mA g^{-1} after 1600 cycles. It was believed that both the nanopores and N-doping provided additional K storage for CNF anodes [107, 108].

Similar to SIBs, the graphitization degree of CNFs also significantly affects the K storage mechanism and rate capability. Tian *et al.* [109] studied the electrochemical performance of highly graphited CNFs in comparison to neat CNFs. It showed that highly graphited CNFs with ordered graphitic layers presented a reversible capacity of 200 mAh g^{-1} at the plateau potential below 0.2V and superior rate performance with a capacity of 226 mAh g^{-1} at 35 C. In contrast, the corresponding values are 62 mAh g^{-1} and 129 mAh g^{-1} for CNFs with amorphous carbon structure.

The superior performance of highly graphitic CNFs was attributed to their high electrical conductivity and layered structure, which are favorable to K ion (de)intercalation reactions.

Electrospun CNF has also been incorporated with transition metal dichalcogenides (TMD, SeS_2, MoSe, MoS_2) for high capacity KIB anodes [110, 111]. TMDs are active to be intercalated with large amounts of K ions; however, large volume expansions during potassiation cause exfoliation and irreversibility of TMDs anodes. TMD nanostructures have been incorporated with strong CNFs to accommodate the volume changes [112]. For example, Zhu *et al.* [113] prepared Cu_2Se/C nanowires anode by electrospinning Cu_2O, PAN and Se mixture into nanofibers, followed by stabilization and carbonization. The 3D flexible network provided fast reaction kinetics and high conductivity to Cu_2Se/C NWs. Consequently, the novel NW anode showed a prolonged cycling life (78 mAh g^{-1} after 1200 cycles) and an impressive rate capacity (104 mAh g^{-1} at 2.0 A g^{-1}).

Alloying anodes present remarkably high theoretical capacities in KIBs (*i.e.*, 225 mAh g^{-1} for Sn, 660 mAh g^{-1} for Sb and 843 mAh g^{-1} for P); however, huge volume expansions (*i.e.*, 400% for Sn) during potassiation cause fracture and failure of alloy anodes [114, 115]. Electrospun CNFs, as a robust platform, has been incorporated with alloy nanoparticles to retain high capacities over long cycles [116]. For instance, Ge *et al.* [117] synthesized a free-standing CNFs/Sb anode for KIBs, where ultrafine Sb particles of approximately 10 nm in size were encapsulated by CNFs (designated as u-Sb@CNFs). The electrospun nanofibers (containing $Sb(Ac)_3$, PAN and PS) were stabilized and heat-treated at 700 ℃, when PS was decomposed to form multichannel and Sb nucleated in PAN-derived CNFs. Hollow nanochannels and ultra-small Sb nanocrystals facilitated K^+ diffusion and strain relaxation during discharge/charge processes. The free-standing u-

Sb@CNFs presented remarkable electrochemical performance with a long cycle life of 2000 cycles and high capacities of over 225 mAh g^{-1} at 1A g^{-1}.

3.3.2 Electrospun nanofibers for cathode

Like Na, K has also been stored intercalation host cathodes, including layered oxides, polyanionic compounds, Prussian blue analogues and organic compounds [104]. Electrospun nanofibers have been used to modify the structural stability and electrochemical behaviors of potential cathodes in KIBs. For layered compound cathodes, SeS_2 was encapsulated into a N-doped porous CNF (SeS_2@NCNFs) via electrospinning [111]. The high N-doping content of CNF was achieved by the heating in NH_3 atmosphere, whereas the low N content was obtained by carbonizing in the reductive N_2/H_2 flow. The pyrrolic and pyridinic N-doping was reported to enhance the chemical affinity of CNFs to K_2Se (the discharge product), indicating stabilized active particles during cycles. The porous structure with abundant empty space would accommodate the volume expansion of SeS_2 as well as facilitate the electrolyte penetration. The robust and conductive CNFs host ensured long cycle life and high energy densities for the SeS_2@NCNFs cathode, namely, a high capacity retention of 85% and 417 mAh g^{-1} after 1000 cycles at 0.5 A g^{-1} with average Coulombic efficiencies near to 100%.

Wang *et al.* [118] designed a Fe/Mn-based layered oxide interconnected NW cathode by electrospinning. The interconnected $K_{0.7}Fe_{0.5}Mn_{0.5}O_2$ NWs not only present a stable 3D network but also possess rapid potassium ion diffusion pathways. In-situ X-ray diffraction patterns showed reversible phase transformation for $K_{0.7}Fe_{0.5}Mn_{0.5}O_2$ during potassiation and depotassiation, indicating excellent reversibility of the cathode material. In a cycling KIBs, the cathode displayed a considerable initial discharge capacity of 178mAh g^{-1} at 20 mA g^{-1}, which was maintained by 70% after 45 cycles (**Figure 10**b). In K-ion full cells, $K_{0.7}Fe_{0.5}Mn_{0.5}O_2$ nanowires//soft carbon

showed a capacity of 119 mAh g^{-1} at 20 mA g^{-1}. At 100 mA g^{-1}, notably, 76% of the initial capacity was retained after 250 cycles, manifesting remarkable cycling stability for K-ion full batteries. During the depotassiation/potassiation processes, the layered skeleton structure ensured excellent stability and reversibility. In addition, compared to dispersed $K_{0.7}Fe_{0.5}Mn_{0.5}O_2$ powder, the interconnect structure presented higher K ion diffusion co-efficiency.

In short, electrospun nanofiber structures have been successfully prepared for the growing KIBs. Similar to SIBs, PAN-based CNFs can be direct utilized as anode materials or host materials to load active particles. In **Table 2**, it is clearly observed that ultra-long life (i.e., 2000 cycles for Sb/CNF anode [117] and 1000 cycles for SeS_2/CNF cathodes [113]) electrodes have been successfully achieved by facile electrospinning, directly evidencing the significance of electrospun nanofibers in promoting the advances of new battery systems. It is also undoubtedly that the research on KIBs electrodes is still at the initial stage, which calls for more efforts in the future to realize the practical application for low-cost KIBs.

3.4 Multivalent-ion battery

Multivalent ion batteries share similar operating mechanisms with monovalent ion batteries but using multivalent charge carriers. The rapid expansion of multivalent ion batteries provides a promising way to overcome the safety, cost and energy density limitations for the state-of-the-art LIB technology. Electrospun nanofiber materials have played essential roles in improving the electrochemical performance of these new battery systems.

3.4.1 Electrospun nanofibers for Zn-ion batteries

Aqueous Zn-ion batteries (ZIBs) have overwhelming advantages in low cost, high safety, and environmental benefit, especially for the non-flammable aqueous electrolyte. Numerous materials like manganese oxides (MnO, MnO_2), Prussian blue analogs, and vanadium-based oxides (*e.g.*,

V_2O_5, $Zn_2V_2O_7$, NaV_3O_8) have been investigated as potential electrodes in ZIBs [119]. Electrospinning provided a veritable method to design smart nanostructures for advanced ZIBs. Chen *et al*. [120] designed a porous V_2O_5 nanofiber by electrospinning using PVP nanofiber template. After calcination, PVP was decomposed, resulting in porous V_2O_5 nanofibers. After the first discharge process, V_2O_5 was transformed into zinc pyrovanadate (ZVO) structure as shown in **Figure 11**a. The new phase with the open framework provided a stable system for the Zn^{2+} insertion/extraction in the following cycles, leading to an excellent discharge capacity of 319 mAh g^{-1} in the 4^{th} cycle and a high reversible capacity 166 mAh g^{-1} at 2 C after 500 cycles(**Figure 11**b,c). Wang *et al.* [16] incorporated $Zn_2V_2O_7$ or V_2O_5 nanoparticles with CNF into metal oxide/CNF core-shell fibers as cathodes for ZIBs. The composites were fabricated by using a dual nozzle electrospinning method. The PAN was used in the outside shell, while PMMA, the oxide precursor, and acetic acid solution were in the internal channel. The electrospun fibers were calcined into the final products of $Zn_2V_2O_7$/CNF or V_2O_5/CNF core/shell structures. Both $Zn_2V_2O_7$ and V_2O_5 in hybrid carbon fibers showed remarkable electrochemical behaviors, for example, both hybrid fibers achieved high capacity retentions of 93.1% ($Zn_2V_2O_7$/CNF) and 95.8% (V_2O_5/CNF) of the initial capacity after an extremely long 2000 cycles at 8 A g^{-1}. The core-shell structure containing carbon matrix and active metal oxides presented excellent conductivity and large surface areas, which facilitated the electron/ion transportation even under high electrode loadings. Zn ion full cells have also been assembled with Zn nanosheet@ CNT anodes, polymer electrolytes and $Zn_2V_2O_7$/CNF or V_2O_5/CNF cathodes. Full cells presented high cyclic capacities of ~400 mAh g^{-1} for V_2O_5/CNF-based full cell and ~200 mAh g^{-1} for $Zn_2V_2O_7$/CN-based full cell, respectively.

Manganese-based oxides with rich polymorphs have been regarded as promising cathodes for aqueous ZIBs; however, the poor electric conductivity and low ion diffusion kinetics for

pristine manganese oxides depressed their performance. To this end, Tang *et al.* [67] prepared N-doped carbon-coated MnO (MnO@N-C) fibers as cathodes in aqueous ZIBs. The Zn storage mechanism was dominated by diffusion-controlled intercalation reactions. MnO@N-C on graphite foil delivered reversible capacities of 176.3 mAh g^{-1}, 100.5 mAh g^{-1} at 0.5 A g^{-1}, 1.2 A g^{-1} after 200 cycles, respectively. A novel core-shell Mn_3O_4/CNF cathode has also been fabricated for ZIBs using a coaxial electrospinning technique [121]. This cathode displayed excellent cycling stability of 225 mAh g^{-1} at 400 mA g^{-1} after 1300 cycles and superior rate capability.

For organic electrodes in ZIBs, Kim *et al.* [122] synthesized polyaniline (PANI)-coated carbon fiber (PANI/CF) cathodes and laser micromachined Zn anodes for ZIBs. Electrospun CNFs were functionalized with hydroxyl groups by HNO_3 before depositing PANI layers on the surface by in-situ polymerization of aniline. The PANI/CF//Zn full cell displayed a discharge capacity 165 mAh g^{-1} at 1 C and an extremely high rate capability of 600C. The full cells could be packaged in different shapes due to the flexibility of PANI/CNF cathodes. A full cell containing 130 μm-thick PANI/CF cathode exhibited an energy density of 159 Wh kg^{-1} and a power density of 16.7 kW kg^{-1}. High power ZIBs have also been delivered another electrospun CNF modified cathode, HCC-V_3S_4 [123], which delivered an energy density of 155.7 Wh kg^{-1} and a power density of 5000 W kg^{-1}.

In addition to aqueous ZIBs, electrospun nanofibers have also been utilized in fabricating all-solid-state ZIBs. Hiralal *et al.* reported an all-solid flexible Zn-C battery [124]. The free-standing CNFs cathode was obtained by annealing electrospun phenolic resin and poly (vinyl butyral). The solid batteries composed of thin zinc foil anodes, MnO/CNT/CNF cathodes and polymer electrolytes. Due to the strong mechanical strength of CNF/CNT network, the battery retained its performance even in high strain conditions. Specifically, there was almost no capacity

fade when bending the all-solid state ZIB from flat to approximately 90°. Electrospun CNF structures have also been widely used in Zn-air batteries systems, for example, FeP/Fe_3O_4/CNF [125], C_9S_8/CNF [126] ,$CuCo_2O_4$/CNF [127], to improve the oxygen electrocatalytic activity and stability.

3.4.2 Electrospun nanofibers for Al-ion battery

Aluminum metal is a high specific capacity (8046 mAh cm^{-3} and 2980 mAh g^{-1}) carrier with low cost, thus endowing rechargeable aluminum-ion batteries (AIBs) with the potential to serve as inexpensive energy storage devices with high energy densities. Another attractive feature for AIBs is the dendrite-free electrodeposition of Al metal, indicating highly safe Al metal batteries. Due to the large ionic radius of 0.535 Å and trivalent nature for Al^{3+}, cathode materials suffer poor cyclic stability and low rate capacities arising from large volume expansions and slow Al^{3+} diffusion. Downsizing the active particles as well as conductive carbon encapsulation have been demonstrated as effective ways to improve the AIBs cathode performance.

TMDs have been applied as high capacity cathodes for AIBs. A conductive 3D N-doped carbon matrix was produced by electrospinning to host $MoSe_2$ nanosheets during the hydrothermal process, forming a flexible $MoSe_2$@NCNF cathode [128]. The N-doped CNF with a large surface area prevented aggregation of $MoSe_2$, resulting in improvement of charge transfer to individual $MoSe_2$ sheet and high utilization of active material for Al storage. Benefiting from the ameliorated nanostructure, the $MoSe_2$@NCNF cathode presented a high capacity of 296.3 mAh g^{-1} at 100 mA g^{-1} and maintained 169.9 mAh g^{-1} after 200 cycles. Through one-pot electrospinning and annealing, Yang *et al.* [129] prepared a free-standing N-CNFs@MoS_2 composite where MoS_2 nanosheets were in-situ formed in CNF by annealing. TEM images revealed that MoS_2 nanocrystals with a thickness of about 5 nm are uniformly dispersed in N-CNFs. The CNFs can provide mechanical

accommodation and electron transfer paths for the MoS_2 nanostructure during the Al ion intercalation/deintercalation. Finally, the freestanding N-CNFs@MoS_2 electrode delivered an initial discharge capacity of 293.2 mAh g^{-1}, and the capacity maintained at 126.6 mAh g^{-1} after 200 circles. Using similar methods, WS_2@CNF [130] and Co_9S_8@CNT–CNF [131] cathodes have also been successfully synthesized with outstanding Al storage performance.

Smart separators have also been prepared by electrospinning for AIBs. Elia *et al.* [132] took use of the electrospun PAN as a separator in AIBs with the 1-ethyl-3-methylimidazolium chloride: aluminum trichloride (EMIMCl: $AlCl_3$) electrolyte. Interestingly, it was observed that the PAN separator significantly affected the dissolution/deposition behaviors of Al, leading to a more homogeneous Al deposition than that of conventional glass fiber separator. This finding is essential to design stable Al metal batteries with high safety and stability. In addition, an Al/graphite full cell using PAN separator was assembled, which presented higher cyclic capacities than these for AIBs with commercial glass fiber separators, offering a testament to the superiority of the electrospun PAN separator for practical applications.

3.4.3 Electrospun nanofibers for Mg -ion battery

Thanks to the high volumetric energy density, the metallic-dendrite-free Mg metal anode and the abundant Mg resources in the earth crust, rechargeable Mg-ion batteries (MIBs) are of significant importance on the path to develop energy storage systems beyond Li-ion batteries. The implementation of MIBs is hindered by several fundamental challenges, such as the absence of suitable electrodes, the unstable electrolyte/electrode interface and the sluggish diffusion kinetics of Mg^{2+} in host materials. Over the past decade, tremendous efforts have been devoted to exploring advanced electrodes for MIBs, among which electrospun nanofiber materials have presented outstanding performance.

Miao *et al.* [133] synthesized V_2MoO_8 cuboids as the Mg cathode by facial electrospinning technology with PVP/NH_4VO_3/$H_{24}Mo_7N_6O_{24}$ precursors, where PVP served as a polymer matrix and NH_4VO_3/$H_{24}Mo_7N_6O_{24}$ as transition metal oxide source. SEM images displayed the continuous and smooth PVP/NH_4VO_3/$H_{24}Mo_7N_6O_{24}$ neat nanofibers, which was calcined into wedged-shaped V_2MoO_8 cuboids at high temperatures, possibly due to the sintering effect. Using all-phenyl-complex electrolyte, at room temperature the V_2MoO_8//Mg cell exhibited an initial capacity of 199.1 mAh g^{-1} with low Coulombic efficiency of 33%. Elevating the temperature to 60 ℃, an initial capacity of 210 mAh g^{-1} with Coulombic efficiency of 94% was obtained. That was because the charge transfer resistance and polarization were greatly decreased at high temperature. However, the capacity fade was still fast due to the irreversible structure changes of V_2MoO_8, requiring more investigations in the future.

The lack of highly ionic conductive and high voltage electrolytes is another key challenge for reliable MIBs. Singh *et al.* [134] prepared an electroactive β-phase PVDF gel polymer electrode using electrospinning. The β-phase PVDF is highly polar and electroactive with a high dipole moment. When immersed in a 0.3M $MgClO_4$ propylene carbonate (PC) solution, the electrospun PVDF nanofibers formed a gel polymer electrolyte, which presented an ionic conductivity of 1.49 mS cm^{-1} at 30 ℃, which value is even higher than that for commercial polypropylene Celgard soaked with $MgClO_4$ PC solution. In addition, the gel polymer electrolyte presented high voltage stability up to 5.0 V vs. Mg^{2+}/Mg, suggesting their suitability to high voltage cathodes. The same group further prepared a PVDF-hexafluoropropylene (HFP) copolymer for MIBs [135]. The β-phase PVDF-co-HFP, as prepared by electrospinning method, is more polar and has a higher affinity towards the polar liquid electrolyte of 0.3M $MgClO_4$ PC than PVDF. Thus, the PVDF-co-HFP presented higher amorphic than PVDF, showing a higher

ionic conductivity of 1.62 mS cm^{-1} and higher voltage stability up to 5.5 V vs. Mg^{2+}/Mg. These results demonstrated that electrospun functional PVDF membranes can be excellent gel polymer electrolyte candidates for MIB applications.

4. Conclusions and perspective

Electrospinning technology has been successfully utilized to design electrodes, separators, and electrolytes of post-Li ion rechargeable batteries for its simplicity and versatility to fabricate nanofiber materials with different structures and components. The functional nanofibers have been adopted to the emerging battery technologies by adjusting the precursor components, electrospinning parameters and thermal treatments. On base of the structures (*i.e.*, porous, hollow, core-shell), functions (*i.e.*, conductive framework, interlayer, anode) and performance of electrospun nanofiber materials applied in post lithium batteries as summarized in **Table 2**, there are many distinctive advantages for the 1D nanostructure by facile electrospinning. ***As host materials***, 1) electrospun CNFs can provide 3D freestanding conductive networks for active materials, resulting in high structure stability, excellent rate capacity, long cyclability and high energy density, especially comparing to the pristine active particles. 2) What is more, CNFs can be flexibly designed with respect to chemical doping, porosity, morphology, graphitization degree and nanostructure, to adapt to different purposes and configurations in batteries. 3) Regarding the surface functional groups on CNFs, such as the heteroatom doping and oxygenated groups, they function as strong chemical immobilizers to polysulfides in LSBs while provide active sites for Na- and K ion storage in SIBs and KIBs. The electrospun nanofiber can be carbonized into CNFs ***as flexible electrodes***, while some are decomposed as sacrificial template for metal oxide nanofibers, such as the V_2O_5 nanofiber for KIBs cathode and $NaCrO_2$ nanowires for SIBs anode. It can be concluded that electrospun nanofibers materials with controllable porosity, chemical

surface and components are ideal platforms to smart electrodes for advanced post-Li ion batteries with high capacities, long life span and low cost for the next generation energy storage applications.

Despite substantial achievements have been obtained by using electrospinning in the energy storage field, there are still some advices for their further development for practical applications in post Li-ion batteries, as following:

(i) Optimization of electrode structure The diameter of electrospun nanofibers is still hardly controlled below 50 nm uniformly, and the smaller diameter of CNFs can offer more efficient electron/ion transport pathways. Besides, porous architecture brings a high surface to volume ratio, which will offer more active sites for reaction. The porous structure and surface chemistry should be adjusted to optimize CNFs to attain high sulfur loading as well as excellent electrochemical performance for LSBs. To systematically build the relationship between pore size and post-lithium-ion batteries system will help structure design to improve the electrochemical performance.

(ii) Freestanding devices Electrospun CNFs have been used as freestanding anodes directly or/and combined with active components (such as Sn, $NaVPO_4F$) as electrodes. These achievements suggest the feasibility of the electrospun CNFs as flexible batteries for soft electronic device applications, which has been rarely reported in post-Li ion batteries so far.

(iii) Chemical doping design Typically, chemical doping can improve the reaction kinetics and provide more absorption/storage/active sites, thus benefiting the electrochemical performance of secondary batteries. However, the detailed working mechanisms for individual heteroatom doping (i.e., N, B, O, P. S) and oxygenated functional groups remain elusive, making it unfeasible to precisely design a optimal nanofiber materials for specific end applications. Besides, the functional groups are believed to be double-edged. On the one hand, there are favorable to provide high capacities or high electronic conductivities; on the other hand, the electrolyte can react with these

functional groups to form thick/unstable solid electrolyte interphase, leading to low coulombic efficiencies. This phenomenon has been widely observed in LIBs, while little research has been conducted to clarify the correlation between the 1st cycle behavior and the nature of surface chemistry in CNF-based electrodes in post Li-ion batteries. In addition, the concentration of chemical doping on CNFs is also essential in determining the electronic structure and electrochemical performance.

(iv) Mass production Electrospinning technology as a simplistic method to fabricate CNFs has been developed for nearly ninety years. The current research on electrospun materials for batteries has still been limited to laboratory-scale. New technologies like multi-nozzle electrospinning, needleless electrospinning have been developed to improve the manufacturing efficiency to promote their practical application in the market, however, the costs to fabricate these delicate nanostructures are still unacceptable. The gap between the achievements in the lab and the requirements for commercial applications is another important issue awaiting to be tackled in the future. The complicated and tedious processes of preparing smart electrospun nanomaterials with low yield in the lab is another challenge for their massive production. Therefore, in addition to the scientific challenges related to the battery performance, the manufacturing feasibility and cost should also be taken into account as it determines whether electrospun nanofiber materials can be practicable to promote the realization of emerging rechargeable batteries in the real market.

Acknowledgment

The work described in this paper was supported by a grant from the Research Committee of The Hong Kong Polytechnic University under project code 1-BE3M.

References

[1] Peng S, Li L, Kong Yoong Lee J, Tian L, Srinivasan M, Adams S, Ramakrishna S. Electrospun carbon nanofibers and their hybrid composites as advanced materials for energy conversion and storage. Nano Energy. 2016; 22: 361-95.
[2] Walter M, Kovalenko MV, Kravchyk KV. Challenges and benefits of post-lithium-ion batteries. New Journal of Chemistry. 2020; 44: 1677-83.
[3] Narins TP. The battery business: lithium availability and the growth of the global electric car industry. The Extractive Industries and Society. 2017; 4: 321-8.
[4] Zubi G, Dufo-Lopez R, Carvalho M, Pasaoglu G. The lithium-ion battery: state of the art and future perspectives. Renewable & Sustainable Energy Reviews. 2018; 89: 292-308.
[5] Yabuuchi N, Kubota K, Dahbi M, Komaba S. Research development on sodium-ion batteries. Chemical Reviews. 2014; 114: 11636-82.
[6] Gao WF, Zhang XH, Zheng XH, Lin X, Cao HB, Zhi Y, Sun Z. Lithium carbonate recovery from cathode scrap of spent lithium-ion battery: a closed-loop process. Environmental Science & Technology. 2017; 51: 1662-9.
[7] Sun YM, Liu NA, Cui Y. Promises and challenges of nanomaterials for lithium-based rechargeable batteries. Nature Energy. 2016; 1: 16071.
[8] Schmuch R, Wagner R, Horpel G, Placke T, Winter M. Performance and cost of materials for lithium-based rechargeable automotive batteries. Nature Energy. 2018; 3: 267-78.
[9] Xu ZL, Kim JK, Kang K. Carbon nanomaterials for advanced lithium sulfur batteries. Nano Today. 2018; 19: 84-107.
[10] Seh ZW, Sun Y, Zhang Q, Cui Y. Designing high-energy lithium-sulfur batteries. Chem Soc Rev. 2016; 45: 5605-34.
[11] Abundance of elements in the earth's crust and in the sea. In: Haynes WM, editor. CRC handbook of chemistry and physics. 97th ed. Boca Raton: CRC Press;; 2016–2017. pp. 14-7.
[12] Liu Q, Wang H, Jiang C, Tang Y. Multi-ion strategies towards emerging rechargeable batteries with high performance. Energy Storage Materials. 2019; 23: 566-86.
[13] Wang FX, Wu XW, Li CY, Zhu YS, Fu LJ, Wu YP, Liu X. Nanostructured positive electrode materials for post-lithium ion batteries. Energy & Environmental Science. 2016; 9: 3570-611.
[14] Reneker DH, Chun I. Nanometre diameter fibres of polymer, produced by electrospinning. Nanotechnology. 1996; 7: 216-23.
[15] Chen Y, Li X, Park K-S, Hong J, Song J, Zhou L, Mai Y-W, Huang H, Goodenough JBJJoMCA. Sulfur encapsulated in porous hollow CNTs@CNFs for high-performance lithium-sulfur batteries. 2014; 2: 10126-30.
[16] Wang H, Zhang S, Deng C. In situ encapsulating metal oxides into core–shell hierarchical hybrid fibers for flexible zinc-ion batteries toward high durability and ultrafast capability for wearable applications. ACS Applied Materials & Interfaces. 2019; 11: 35796-808.
[17] Gong Z, Wu Q, Wang F, Li X, Fan X, Yang H, Luo Z. A hierarchical micro/mesoporous carbon fiber/sulfur composite for high-performance lithium–sulfur batteries. RSC Advances. 2016; 6: 37443-51.
[18] Li YF, Li QH, Tan ZC. A review of electrospun nanofiber-based separators for rechargeable lithium-ion batteries. Journal of Power Sources. 2019; 443: 227262.
[19] Li C, Qin B, Zhang Y, Varzi A, Passerini S, Wang J, Dong J, Zeng D, Liu Z, Cheng H. Single-ion conducting electrolyte based on electrospun nanofibers for high-performance lithium batteries. Advanced Energy Materials. 2019; 9: 1803422.
[20] Weng W, Kurihara R, Wang J, Shiratori S. Electrospun carbon nanofiber-based composites for lithium-ion batteries: Structure optimization towards high performance. Composites Communications. 2019; 15: 135-48.
[21] Li W, Li M, Adair KR, Sun X, Yu Y. Carbon nanofiber-based nanostructures for lithium-ion and sodium-ion batteries. Journal of Materials Chemistry A. 2017; 5: 13882-906.
[22] Klein KL, Melechko AV, McKnight TE, Retterer ST, Rack PD, Fowlkes JD, Joy DC, Simpson ML. Surface characterization and functionalization of carbon nanofibers. Journal of Applied Physics. 2008; 103: 061301.

[23] Li X, Chen Y, Huang H, Mai Y-W, Zhou L. Electrospun carbon-based nanostructured electrodes for advanced energy storage – A review. Energy Storage Materials. 2016; 5: 58-92.
[24] Subbiah T, Bhat GS, Tock RW, Parameswaran S, Ramkumar SS. Electrospinning of nanofibers. Journal of Applied Polymer Science. 2005; 96: 557-69.
[25] Li D, Xia Y. Electrospinning of nanofibers: reinventing the wheel? Advanced Materials. 2004; 16: 1151-70.
[26] Bubakir MM, Li H, Barhoum A, Yang W. Advances in melt electrospinning technique. Handbook of Nanofibers. Ahmed Barhoum, Mikhael Bechelany, Abdel Salam Hamdy Makhlouf ed. Switzerland: Springer, Cham; 2018. pp. 1-32.
[27] S. Rafiei SM, B. Noroozi, V. Mottaghitable and A. K. Haghi. Mathematical modeling in electrospinning process of nanofibers: a detailed review. Cellulose Chemistry and Technology 2013; 47(5): 323-38.
[28] Lei T, Chen W, Hu Y, Lv W, Lv X, Yan Y, Huang J, Jiao Y, Chu J, Yan C, Wu C, Li Q, He W, Xiong J. A nonflammable and thermotolerant separator suppresses polysulfide dissolution for safe and long-cycle lithium-sulfur batteries. Advanced Energy Materials. 2018; 8: 1802441.
[29] Xu ZL, Huang JQ, Chong WG, Qin XY, Wang XY, Zhou LM, Kim JK. In situ TEM study of volume expansion in porous carbon nanofiber/sulfur cathodes with exceptional high-rate performance. Advanced Energy Materials. 2017; 7: 1602078.
[30] Han H, Chen X, Qian J, Zhong F, Feng X, Chen W, Ai X, Yang H, Cao Y. Hollow carbon nanofibers as high-performance anode materials for sodium-ion batteries. Nanoscale. 2019; 11: 21999-2005.
[31] Huang J-Q, Zhang B, Xu Z-L, Abouali S, Akbari Garakani M, Huang J, Kim J-K. Novel interlayer made from Fe_3C/carbon nanofiber webs for high performance lithium–sulfur batteries. Journal of Power Sources. 2015; 285: 43-50.
[32] Xu Z-L, Yao S, Cui J, Zhou L, Kim J-K. Atomic scale amorphous FeO_x/carbon nanofiber anodes for Li-ion and Na-ion batteries. Energy Storage Materials. 2017; 8: 10-9.
[33] Ji L, Rao M, Aloni S, Wang L, Cairns EJ, Zhang Y. Porous carbon nanofiber–sulfur composite electrodes for lithium/sulfur cells. Energy & Environmental Science. 2011; 4: 5053-9.
[34] Zhang B, Kang F, Tarascon J-M, Kim J-K. Recent advances in electrospun carbon nanofibers and their application in electrochemical energy storage. Progress in Materials Science. 2016; 76: 319-80.
[35] Mao X, Hatton T, Rutledge G. A review of electrospun carbon fibers as electrode materials for energy storage. Current Organic Chemistry. 2013; 17: 1390-401.
[36] Manop Panapoy ADBK. Electrical conductivity of PAN-based cabon nanofibers prepared by electrospinning method. Thammasat Int. J. Sc. Tech. 2008; 13 Special Edition: 11-7.
[37] Hu J, Xu Z, Li X, Liang S, Chen Y, Lyu L, Yao H, Lu Z, Zhou L. Partially graphitic hierarchical porous carbon nanofiber for high performance supercapacitors and lithium ion batteries. Journal of Power Sources. 2020; 462: 228098.
[38] Hu J, Wang Z, Fu Y, Lyu L, Lu Z, Zhou L. In situ assembly of MnO_2 nanosheets on sulfur-embedded multichannel carbon nanofiber composites as cathodes for lithium-sulfur batteries. Science China Materials. 2020; 63: 728-38.
[39] Lin L, Pei F, Peng J, Fu A, Cui J, Fang X, Zheng N. Fiber network composed of interconnected yolk-shell carbon nanospheres for high-performance lithium-sulfur batteries. Nano Energy. 2018; 54: 50-8.
[40] Li Z, Zhang JT, Chen YM, Li J, Lou XW. Pie-like electrode design for high-energy density lithium-sulfur batteries. Nat Commun. 2015; 6: 8850.
[41] Liang G, Wu J, Qin X, Liu M, Li Q, He YB, Kim JK, Li B, Kang F. Ultrafine TiO_2 decorated carbon nanofibers as multifunctional interlayer for high-performance lithium-sulfur battery. ACS Appl Mater Interfaces. 2016; 8: 23105-13.
[42] Wang H, Zhang B, Zeng X, Yan L, Zheng J, Ling M, Hou Y, Lu Y, Liang C. 3D porous carbon nanofibers with CeO_2-decorated as cathode matrix for high performance lithium-sulfur batteries. Journal of Power Sources. 2020; 473: 228588.

[43] Zhen Li YJ, Lixia Yuan, Ziqi Yi, Chao Wu,Yang Liu, Peter Strasser, and Yunhui Huang. A highly ordered meso@microporous carbon-supported sulfur@smaller sulfur core-shell structured cathode for Li-S batteries. ACS Nano. 2014; 8(9): 9295–303.
[44] Lee JS, Kim W, Jang J, Manthiram A. Sulfur-embedded activated multichannel carbon nanofiber composites for long-life, high-rate lithium-sulfur batteries. Advanced Energy Materials. 2017; 7: 1601943.
[45] Rahaman MSA, Ismail AF, Mustafa A. A review of heat treatment on polyacrylonitrile fiber. Polymer Degradation and Stability. 2007; 92: 1421-32.
[46] Xu ZL, Lin S, Onofrio N, Zhou L, Shi F, Lu W, Kang K, Zhang Q, Lau SP. Exceptional catalytic effects of black phosphorus quantum dots in shuttling-free lithium sulfur batteries. Nat Commun. 2018; 9: 4164.
[47] Wu F, Shi LL, Mu DB, Xu HL, Wu BR. A hierarchical carbon fiber/sulfur composite as cathode material for Li-S batteries. Carbon. 2015; 86: 146-55.
[48] Yao SS, Guo RD, Xie FW, Wu ZZ, Gao KD, Zhang CJ, Shen XQ, Li TB, Qin SB. Electrospun three-dimensional cobalt decorated nitrogen doped carbon nanofibers network as freestanding electrode for lithium/sulfur batteries. Electrochimica Acta. 2020; 337: 135765.
[49] Zhang YX, Wang PP, Tan H, Fan XY, Huang K. Free-standing sulfur and graphitic porous carbon nanofibers composite cathode for high electrochemical performance of lithium-sulfur batteries. Journal of the Electrochemical Society. 2018; 165: A741-A5.
[50] Li X, Fu N, Zou J, Zeng X, Chen Y, Zhou L, Huang H. Sulfur-impregnated N-doped hollow carbon nanofibers as cathode for lithium-sulfur batteries. Materials Letters. 2017; 209: 505-8.
[51] Song X, Wang S, Bao Y, Liu G, Sun W, Ding L-X, Liu H, Wang H. A high strength, free-standing cathode constructed by regulating graphitization and the pore structure in nitrogen-doped carbon nanofibers for flexible lithium–sulfur batteries. Journal of Materials Chemistry A. 2017; 5: 6832-9.
[52] Zeng L, Pan F, Li W, Jiang Y, Zhong X, Yu Y. Free-standing porous carbon nanofibers-sulfur composite for flexible Li-S battery cathode. Nanoscale. 2014; 6: 9579-87.
[53] Zhang YZ, Zhang Z, Liu S, Li GR, Gao XP. Free-standing porous carbon nanofiber/carbon nanotube film as sulfur immobilizer with high areal capacity for lithium-sulfur battery. ACS Appl Mater Interfaces. 2018; 10: 8749-57.
[54] Deng N, Kang W, Ju J, Fan L, Zhuang X, Ma X, He H, Zhao Y, Cheng B. Polyvinyl alcohol-derived carbon nanofibers/carbon nanotubes/sulfur electrode with honeycomb-like hierarchical porous structure for the stable-capacity lithium/sulfur batteries. Journal of Power Sources. 2017; 346: 1-12.
[55] Deng NP, Ju JG, Yan J, Zhou XH, Qin QQ, Zhang K, Liang YY, Li QX, Kang WM, Cheng BW. CeF_3-doped porous carbon nanofibers as sulfur immobilizers in cathode material for high-performance lithium-sulfur batteries. Acs Applied Materials & Interfaces. 2018; 10: 12626-38.
[56] Chu RX, Lin J, Wu CQ, Zheng J, Chen YL, Zhang J, Han RH, Zhang Y, Guo H. Reduced graphene oxide coated porous carbon-sulfur nanofiber as a flexible paper electrode for lithium-sulfur batteries. Nanoscale. 2017; 9: 9129-38.
[57] Han S, Pu X, Li X, Liu M, Li M, Feng N, Dou S, Hu W. High areal capacity of Li-S batteries enabled by freestanding CNF/rGO electrode with high loading of lithium polysulfide. Electrochimica Acta. 2017; 241: 406-13.
[58] Liang Y, Deng N, Ju J, Zhou X, Yan J, Zhong C, Kang W, Cheng B. Facilitation of lithium polysulfides adsorption by nitrogen doped carbon nanofibers with 3D interconnected pore structures for high-stable lithium-sulfur batteries. Electrochimica Acta. 2018; 281: 257-65.
[59] Ma XZ, Jin B, Wang HY, Hou JZ, Zhong XB, Wang HH, Xin PM. S–TiO_2 composite cathode materials for lithium/sulfur batteries. Journal of Electroanalytical Chemistry. 2015; 736: 127-31.
[60] Ye J, He F, Nie J, Cao Y, Yang H, Ai X. Sulfur/carbon nanocomposite-filled polyacrylonitrile nanofibers as a long life and high capacity cathode for lithium–sulfur batteries. Journal of Materials Chemistry A. 2015; 3: 7406-12.
[61] Kalybekkyzy S, Mentbayeva A, Kahraman MV, Zhang Y, Bakenov Z. Flexible S/DPAN/KB nanofiber composite as binder-free cathodes for Li-S batteries. Journal of The Electrochemical Society. 2019; 166: A5396-A402.

[62] Kim JH, Choi J, Seo J, Kwon J, Paik U. Two-dimensional Nafion nanoweb anion-shield for improved electrochemical performances of lithium–sulfur batteries. Journal of Materials Chemistry A. 2016; 4: 11203-6.
[63] Zhu X, Ouyang Y, Chen J, Zhu X, Luo X, Lai F, Zhang H, Miao Y-E, Liu T. In situ extracted poly(acrylic acid) contributing to electrospun nanofiber separators with precisely tuned pore structures for ultra-stable lithium–sulfur batteries. Journal of Materials Chemistry A. 2019; 7: 3253-63.
[64] Su YS, Manthiram A. Lithium-sulphur batteries with a microporous carbon paper as a bifunctional interlayer. Nat Commun. 2012; 3: 1166.
[65] Singhal R, Chung S-H, Manthiram A, Kalra V. A free-standing carbon nanofiber interlayer for high-performance lithium–sulfur batteries. Journal of Materials Chemistry A. 2015; 3: 4530-8.
[66] Yao SS, Tang H, Liu MQ, Chen LL, Jing MX, Shen XQ, Li TB, Tan JL. TiO_2 nanoparticles incorporation in carbon nanofiber as a multifunctional interlayer toward ultralong cycle-life lithium-sulfur batteries. Journal of Alloys and Compounds. 2019; 788: 639-48.
[67] Tang F, He T, Zhang H, Wu X, Li Y, Long F, Xiang Y, Zhu L, Wu J, Wu X. The MnO@N-doped carbon composite derived from electrospinning as cathode material for aqueous zinc ion battery. Journal of Electroanalytical Chemistry. 2020; 873: 114368.
[68] Wang ML, Song YZ, Sun ZT, Shao YL, Wei CH, Xia Z, Tian ZN, Liu ZF, Sun JY. Conductive and catalytic VTe_2@MgO heterostructure as effective polysulfide promotor for lithium-sulfur batteries. Acs Nano. 2019; 13: 13235-43.
[69] Zhuang R, Yao S, Shen X, Li T. A freestanding MoO_2-decorated carbon nanofibers interlayer for rechargeable lithium sulfur battery. International Journal of Energy Research. 2019; 43: 1111-20.
[70] Rao M, Geng X, Li X, Hu S, Li W. Lithium-sulfur cell with combining carbon nanofibers–sulfur cathode and gel polymer electrolyte. Journal of Power Sources. 2012; 212: 179-85.
[71] Zhu P, Zhu JD, Zang J, Chen C, Lu Y, Jiang MJ, Yan CY, Dirican M, Selvan RK, Zhang XW. A novel bi-functional double-layer rGO-PVDF/PVDF composite nanofiber membrane separator with enhanced thermal stability and effective polysulfide inhibition for high-performance lithium-sulfur batteries. Journal of Materials Chemistry A. 2017; 5: 15096-104.
[72] Gupta A, Sivaram S. Separator membranes for lithium–sulfur batteries: design principles, structure, and performance. Energy Technology. 2019; 7: 1800819.
[73] Zhou C, He Q, Li Z, Meng J, Hong X, Li Y, Zhao Y, Xu X, Mai L. A robust electrospun separator modified with in situ grown metal-organic frameworks for lithium-sulfur batteries. Chemical Engineering Journal. 2020; 395: 124979.
[74] Wang XE, Girard GMA, Zhu HJ, Yunis R, MacFarlane DR, Mecerreyes D, Bhattacharyya AJ, Howlett PC, Forsyth M. Poly(ionic liquid)s/electrospun nanofiber composite polymer electrolytes for high energy density and safe Li metal batteries. Acs Applied Energy Materials. 2019; 2: 6237-45.
[75] Liang Z, Zheng GY, Liu C, Liu N, Li WY, Yan K, Yao HB, Hsu PC, Chu S, Cui Y. Polymer nanofiber-guided uniform lithium deposition for battery electrodes. Nano Letters. 2015; 15: 2910-6.
[76] Li CC, Qin BS, Zhang YF, Varzi A, Passerini S, Wang JY, Dong JM, Zeng DL, Liu ZH, Cheng HS. Single-Ion conducting electrolyte based on electrospun nanofibers for high-performance lithium batteries. Advanced Energy Materials. 2019; 9: 201803422.
[77] Fang Y, Yu X-Y, Lou XW. Nanostructured electrode materials for advanced sodium-Ion batteries. Matter. 2019; 1: 90-114.
[78] Lin D, Li K, Wang Q, Lyu L, Li B, Zhou L. Rate-independent and ultra-stable low-temperature sodium storage in pseudocapacitive TiO_2 nanowires. Journal of Materials Chemistry A. 2019; 7: 19297-304.
[79] Zhao X, Luo M, Zhao WX, Xu RM, Liu Y, Shen H. SnO_2 Nanosheets Anchored on a 3D, Bicontinuous Electron and Ion Transport Carbon Network for High-Performance Sodium-Ion Batteries. Acs Applied Materials & Interfaces. 2018; 10: 38006-14.
[80] Zhang DM, Jia JH, Yang CC, Jiang Q. Fe_7Se_8 nanoparticles anchored on N-doped carbon nanofibers as high-rate anode for sodium-ion batteries. Energy Storage Materials. 2020; 24: 439-49.

[81] Li W, Bi R, Liu G, Tian Y, Zhang L. 3D Interconnected MoS_2 with enlarged interlayer spacing grown on carbon nanofibers as a flexible anode toward superior sodium-ion batteries. ACS Appl Mater Interfaces. 2018; 10: 26982-9.
[82] Liu M, Zhang P, Qu Z, Yan Y, Lai C, Liu T, Zhang S. Conductive carbon nanofiber interpenetrated graphene architecture for ultra-stable sodium ion battery. Nat Commun. 2019; 10: 3917.
[83] Wang Y, Liu Y, Liu Y, Shen Q, Chen C, Qiu F, Li P, Jiao L, Qu X. Recent advances in electrospun electrode materials for sodium-ion batteries. Journal of Energy Chemistry. 2021; 54: 225-41.
[84] Xu ZL, Park J, Yoon C, Kim H, Kang K. Graphitic Carbon Materials for Advanced Sodium-Ion Batteries. Small Methods. 2019; 3: 201800227.
[85] Xu ZL, Yoon G, Park KY, Park H, Tamwattana O, Kim SJ, Seong WM, Kang K. Tailoring sodium intercalation in graphite for high energy and power sodium ion batteries. Nature Communications. 2019; 10: 2598
[86] Zhang B, Ghimbeu CM, Laberty C, Vix-Guterl C, Tarascon J-M. Correlation between microstructure and Na storage behavior in hard carbon. Advanced Energy Materials. 2016; 6: 1501588.
[87] Alvin S, Cahyadi HS, Hwang J, Chang W, Kwak SK, Kim J. Revealing the intercalation mechanisms of lithium, sodium, and potassium in hard carbon. Advanced Energy Materials. 2020; 10: 202000283.
[88] Saurel D, Orayech B, Xiao BW, Carriazo D, Li XL, Rojo T. From charge storage mechanism to performance: a roadmap toward high specific energy sodium-ion batteries through carbon anode optimization. Advanced Energy Materials. 2018; 8: 1703268.
[89] Shan C, Feng X, Yang J, Yang X, Guan H-Y, Argueta M, Wu X-L, Liu D-S, Austin DJ, Nie P, Yue Y. Hierarchical porous carbon pellicles: electrospinning synthesis and applications as anodes for sodium-ion batteries with an outstanding performance. Carbon. 2020; 157: 308-15.
[90] Ma M, Yao Y, Wu Y, Yu Y. Progress and prospects of transition metal sulfides for sodium storage. Advanced Fiber Materials. 2020: https://doi.org/10.1007/s42765-020-00052-w.
[91] Wang R, Chen S, Ren D, Liu S, He B, Gong Y, Wang H. Plasma treated TiO_2/C nanofibers as high performance anode materials for sodium-ion batteries. RSC Advances. 2019; 9: 18451-8.
[92] Wang L, Wei Z, Mao M, Wang H, Li Y, Ma J. Metal oxide/graphene composite anode materials for sodium-ion batteries. Energy Storage Materials. 2019; 16: 434-54.
[93] Liu Q, Hu Z, Chen M, Zou C, Jin H, Wang S, Chou SL, Dou SX. Recent progress of layered transition metal oxide cathodes for sodium-ion batteries. Small. 2019; 15: 1805381.
[94] Liu Y, Shen Q, Zhao X, Zhang J, Liu X, Wang T, Zhang N, Jiao L, Chen J, Fan LZ. Hierarchical engineering of porous P2-$Na_{2/3}Ni_{1/3}Mn_{2/3}O_2$ nanofibers assembled by nanoparticles enables superior sodium-ion storage cathodes. Advanced Functional Materials. 2019; 30: 1907837.
[95] Liang L, Sun X, Denis DK, Zhang J, Hou L, Liu Y, Yuan C. Ultralong layered $NaCrO_2$ nanowires: a competitive wide-temperature-operating cathode for extraordinary high-rate sodium-ion batteries. ACS Appl Mater Interfaces. 2019; 11: 4037-46.
[96] Jin T, Liu Y, Li Y, Cao K, Wang X, Jiao L. Electrospun $NaVPO_4F$/C nanofibers as self-standing cathode material for ultralong cycle life Na-ion batteries. Advanced Energy Materials. 2017; 7: 1700087.
[97] Wang F, Zhang N, Zhao X, Wang L, Zhang J, Wang T, Liu F, Liu Y, Fan LZ. Realizing a high-performance na-storage cathode by tailoring ultrasmall Na_2FePO_4F nanoparticles with facilitated reaction kinetics. Adv Sci (Weinh). 2019; 6: 1900649.
[98] Kajiyama S, Kikkawa J, Hoshino J, Okubo M, Hosono E. Assembly of $Na_3V_2(PO_4)_3$ nanoparticles confined in a one-dimensional carbon sheath for enhanced sodium-ion cathode properties. Chemistry-a European Journal. 2014; 20: 12636-40.
[99] Li H, Bai Y, Wu F, Li Y, Wu C. Budding willow branches shaped $Na_3V_2(PO_4)_3$/C nanofibers synthesized via an electrospinning technique and used as cathode material for sodium ion batteries. Journal of Power Sources. 2015; 273: 784-92.
[100] Hu Y, Wu L, Liao GX, Yang Y, Ye F, Chen JB, Zhu X, Zhong SK. Electrospinning synthesis of Na_2MnPO_4F/C nanofibers as a high voltage cathode material for Na-ion batteries. Ceramics International. 2018; 44: 17577-84.

[101] Zhijiang C, Qing Z, Cong Z, Xianyou S, Yuanpei L. Development of a sodium/electrospun poly(5-cyanoindole) nanofiber secondary battery system with high performance. Synthetic Metals. 2017; 231: 15-8.
[102] Janakiraman S, Surendran A, Ghosh S, Anandhan S, Venimadhav A. Electroactive poly(vinylidene fluoride) fluoride separator for sodium ion battery with high coulombic efficiency. Solid State Ionics. 2016; 292: 130-5.
[103] Janakiraman S, Surendran A, Biswal R, Ghosh S, Anandhan S, Venimadhav A. Electrospun electroactive polyvinylidene fluoride-based fibrous polymer electrolyte for sodium ion batteries. Materials Research Express. 2019; 6: 086318.
[104] Zhang WC, Liu YJ, Guo ZP. Approaching high-performance potassium-ion batteries via advanced design strategies and engineering. Science Advances. 2019; 5: eaav7412.
[105] Lei K-X, Wang J, Chen C, Li S-Y, Wang S-W, Zheng S-J, Li F-J. Recent progresses on alloy-based anodes for potassium-ion batteries. Rare Metals. 2020; 39: 989-1004.
[106] Zhao X, Xiong P, Meng J, Liang Y, Wang J, Xu Y. High rate and long cycle life porous carbon nanofiber paper anodes for potassium-ion batteries. J. Mater. Chem. A. 2017; 5: 19237-44.
[107] Yang W, Zhou J, Wang S, Zhang W, Wang Z, Lv F, Wang K, Sun Q, Guo S. Freestanding film made by necklace-like N-doped hollow carbon with hierarchical pores for high-performance potassium-ion storage. Energy & Environmental Science. 2019; 12: 1605-12.
[108] Adams RA, Syu JM, Zhao Y, Lo CT, Varma A, Pol VG. Binder-free N- and O-rich carbon nanofiber anodes for long cycle life K-ion batteries. ACS Appl Mater Interfaces. 2017; 9: 17872-81.
[109] Tian S, Jiang Q, Cai T, Wang Y, Wang D, Kong D, Ren H, Zhou J, Xing W. Graphitized electrospun carbon fibers with superior cyclability as a free-standing anode of potassium-ion batteries. Journal of Power Sources. 2020; 474: 228479.
[110] Shen Q, Jiang P, He H, Chen C, Liu Y, Zhang M. Encapsulation of $MoSe_2$ in carbon fibers as anodes for potassium ion batteries and nonaqueous battery-supercapacitor hybrid devices. Nanoscale. 2019; 11: 13511-20.
[111] Yao Y, Xu R, Chen M, Cheng X, Zeng S, Li D, Zhou X, Wu X, Yu Y. Encapsulation of SeS_2 into nitrogen-doped free-standing carbon nanofiber film enabling long cycle life and high energy density K-SeS2 battery. ACS Nano. 2019; 13: 4695-704.
[112] Tian Z, Chui N, Lian R, Yang Q, Wang W, Yang C, Rao D, Huang J, Zhang Y, Lai F, Liu C, Liu T. Dual anionic vacancies on carbon nanofiber threaded MoSSe arrays: a free-standing anode for high-performance potassium-ion storage. Energy Storage Materials. 2020; 27: 591-8.
[113] Zhu X, Gao J, Li J, Hu G, Li J, Zhang G, Xiang B. Self-supporting N-rich Cu_2Se/C nanowires for highly reversible, long-life potassium-ion storage. Sustainable Energy & Fuels. 2020; 4: 2453-61.
[114] Song K, Liu C, Mi L, Chou S, Chen W, Shen C. Recent progress on the alloy-based anode for sodium-ion batteries and potassium-ion batteries. Small. 2019: https://doi.org/10.1002/smll.201903194.
[115] Loaiza LC, Monconduit L, Seznec V. Si and Ge-based anode materials for Li-, Na-, and K-ion batteries: a perspective from structure to electrochemical mechanism. Small. 2020; 16: 1905260.
[116] Wu Y, Hu S, Xu R, Wang J, Peng Z, Zhang Q, Yu Y. Boosting potassium-ion battery performance by encapsulating red phosphorus in free-standing nitrogen-doped porous hollow carbon nanofibers. Nano Lett. 2019; 19: 1351-8.
[117] Ge X, Liu S, Qiao M, Du Y, Li Y, Bao J, Zhou X. Enabling superior electrochemical properties for highly efficient potassium storage by impregnating ultrafine Sb nanocrystals within nanochannel-containing carbon nanofibers. Angew Chem Int Ed Engl. 2019; 58: 14578-83.
[118] Wang X, Xu X, Niu C, Meng J, Huang M, Liu X, Liu Z, Mai L. Earth Abundant Fe/Mn-based layered oxide interconnected nanowires for advanced K-ion full batteries. Nano Lett. 2017; 17: 544-50.
[119] Blanc LE, Kundu D, Nazar LF. Scientific Challenges for the Implementation of Zn-Ion Batteries. Joule. 2020; 4: 771-99.
[120] Chen X, Wang L, Li H, Cheng F, Chen J. Porous V_2O_5 nanofibers as cathode materials for rechargeable aqueous zinc-ion batteries. Journal of Energy Chemistry. 2019; 38: 20-5.

[121] Long J, Yang Z, Yang F, Cuan J, Wu J. Electrospun core-shell Mn_3O_4/carbon fibers as high-performance cathode materials for aqueous zinc-ion batteries. Electrochimica Acta. 2020; 344: 136155.
[122] Kim C, Ahn BY, Wei T-S, Jo Y, Jeong S, Choi Y, Kim I-D, Lewis JA. High-power aqueous zinc-ion batteries for customized electronic devices. ACS Nano. 2018; 12: 11838-46.
[123] Liu S, Chen X, Zhang Q, Zhou J, Cai Z, Pan A. Fabrication of an inexpensive hydrophilic bridge on a carbon substrate and loading vanadium sulfides for flexible aqueous zinc-ion batteries. ACS Applied Materials & Interfaces. 2019; 11: 36676-84.
[124] Hiralal P, Imaizumi S, Unalan HE, Matsumoto H, Minagawa M, Rouvala M, Tanioka A, Amaratunga GAJ. Nanomaterial-enhanced all-solid flexible Zinc-carbon batteries. Acs Nano. 2010; 4: 2730-4.
[125] Wang M, Zhang C, Meng T, Pu Z, Jin H, He D, Zhang J, Mu S. Iron oxide and phosphide encapsulated within N,P-doped microporous carbon nanofibers as advanced tri-functional electrocatalyst toward oxygen reduction/evolution and hydrogen evolution reactions and zinc-air batteries. Journal of Power Sources. 2019; 413: 367-75.
[126] Peng W, Wang Y, Yang XX, Mao LC, Jin JH, Yang SL, Fu K, Li G. Co_9S_8 nanoparticles embedded in multiple doped and electrospun hollow carbon nanofibers as bifunctional oxygen electrocatalysts for rechargeable zinc-air battery. Applied Catalysis B-Environmental. 2020; 268: 118437.
[127] Wang XJ, Li Y, Jin T, Meng J, Jiao LF, Zhu M, Chen J. Electrospun thin-walled $CuCo_2O_4$@C nanotubes as bifunctional oxygen electrocatalysts for rechargeable Zn-air batteries. Nano Letters. 2017; 17: 7989-94.
[128] Yang W, Lu H, Cao Y, Jing P, Hu X, Yu H. A flexible free-standing cathode based on graphene-like $MoSe_2$ nanosheets anchored on N-doped carbon nanofibers for rechargeable aluminum-ion batteries. Ionics. 2020; 26: 3405-13.
[129] Yang W, Lu H, Cao Y, Xu B, Deng Y, Cai W. Flexible free-standing MoS_2/carbon nanofibers composite cathode for rechargeable aluminum-ion batteries. ACS Sustainable Chemistry & Engineering. 2019; 7: 4861-7.
[130] Yang WW, Lu HM, Cao Y, Jing PC. Single-/few-layered ultrasmall WS_2 nanoplates embedded in nitrogen-doped carbon nanofibers as a cathode for rechargeable aluminum batteries. Journal of Power Sources. 2019; 441: 227173.
[131] Hu Y, Ye D, Luo B, Hu H, Zhu X, Wang S, Li L, Peng S, Wang L. A binder-free and free-standing cobalt sulfide@carbon nanotube cathode material for aluminum-ion batteries. Adv Mater. 2018; 30: 1703824
[132] Elia GA, Ducros JB, Sotta D, Delhorbe V, Brun A, Marquardt K, Hahn R. Polyacrylonitrile separator for high-performance aluminum batteries with improved interface stability. ACS Appl Mater Interfaces. 2017; 9: 38381-9.
[133] Miao X, Chen Z, Wang N, Nuli Y, Wang J, Yang J, Hirano S-i. Electrospun V_2MoO_8 as a cathode material for rechargeable batteries with Mg metal anode. Nano Energy. 2017; 34: 26-35.
[134] Singh R, Janakiraman S, Khalifa M, Anandhan S, Ghosh S, Venimadhav A, Biswas K. An electroactive β-phase polyvinylidene fluoride as gel polymer electrolyte for magnesium–ion battery application. Journal of Electroanalytical Chemistry. 2019; 851: 113417.
[135] Singh R, Janakiraman S, Agrawal A, Ghosh S, Venimadhav A, Biswas K. An amorphous poly(vinylidene fluoride-co-hexafluoropropylene) based gel polymer electrolyte for magnesium ion battery. Journal of Electroanalytical Chemistry. 2020; 858: 113788.

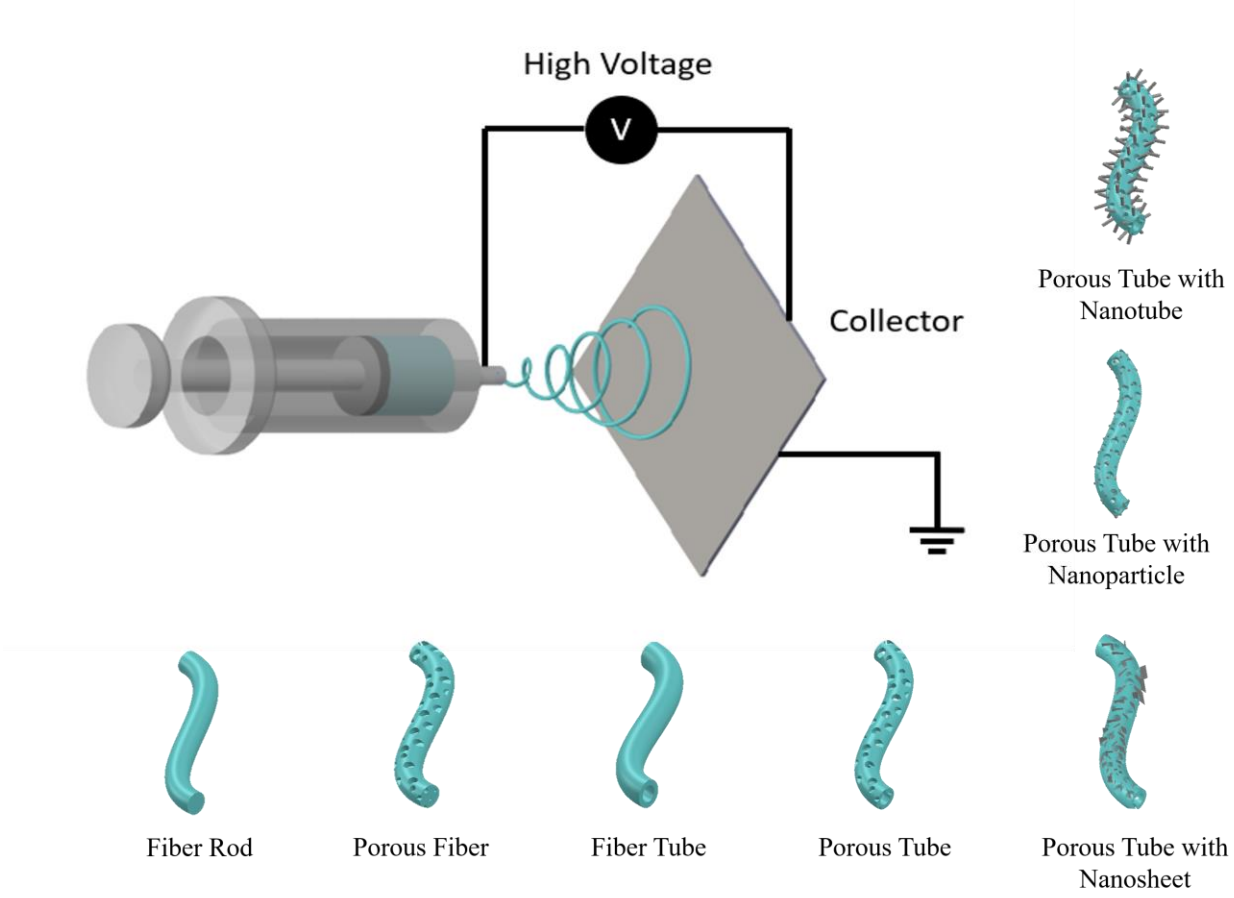

1

2 **Figure 1** The process of electrospinning and the different structure of electrpun nanofibers.

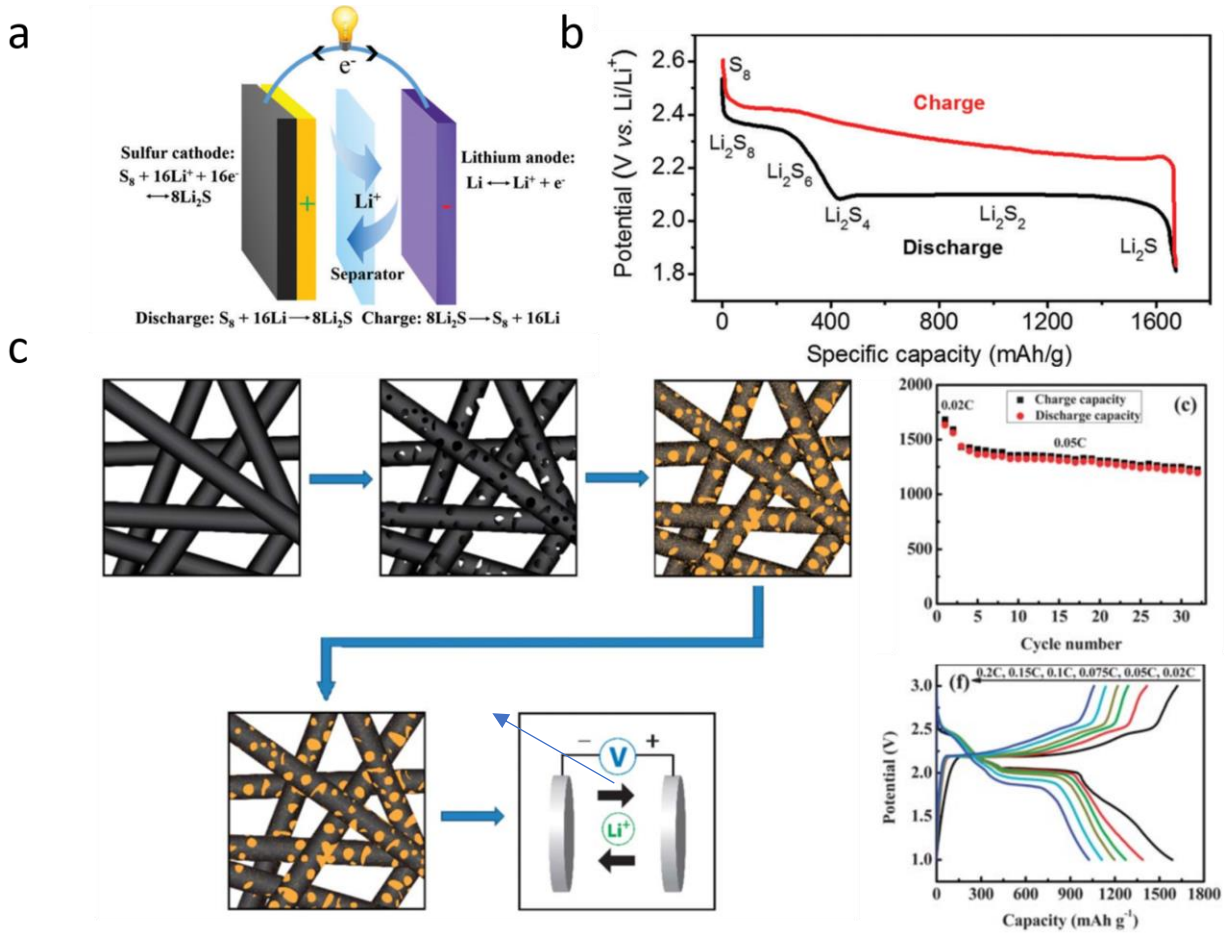

Figure 2 (a) Schematic illustration of the lithium and sulfur electrochemistry, (b) the theoretical charge/discharge curve of lithium sulfur batteries in ether-based electrolytes [10]. Copyright 2016, the Royal Society of Chemistry. (c) Schematic illustration of the process to prepare porous carbon nanofiber/sulfur cathode; galvanostatic charge/discharge profiles and reversible capacity vs. current density [33]. Copyright 2011, The Royal Society of Chemistry.

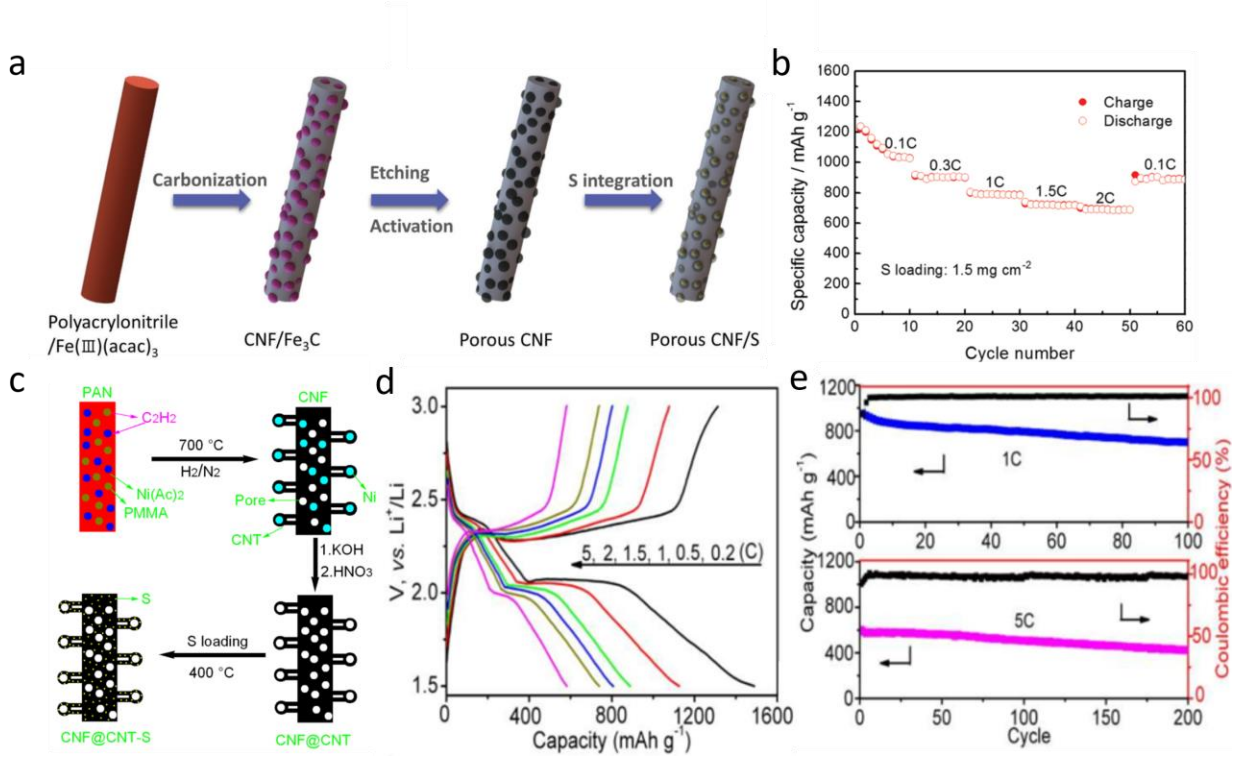

Figure 3 (a) Preparation of porous carbon nanofiber/sulfur cathode, (b) rate capacities of the porous carbon nanofiber/sulfur electrode from 0.1 C to 2 C [29]. Copyright 2017, WILEY-VCH. (c) Schematic illustration of the preparation processes of the carbon nanotubes @carbon nanofibers-sulfur cathode, (d, e) electrochemical performance of cathode [15]. Copyright 2014, The Royal Society of Chemistry.

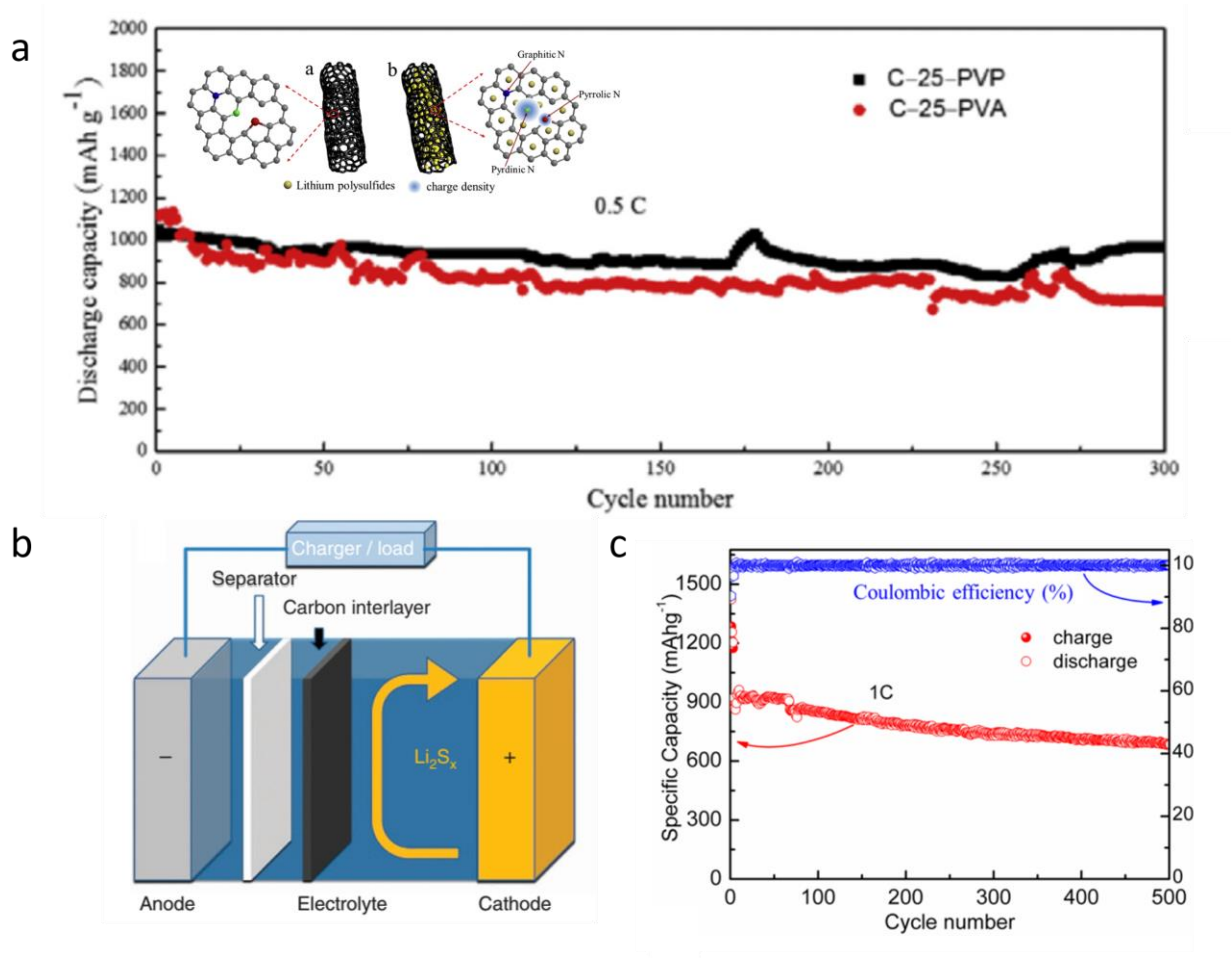

Figure 4 (a) Schematic of nitrogen-doped carbon nanofibers and electrochemical performance of nitrogen-doped porous carbon nanofibers/sulfur and porous carbon nanofibers/sulfur [58]. Copyright 2018, Elsevier. (b) Schematic configuration of lithium-sulfur batteries with interlayer [64]. Copyright 2012, Macmillan Publishers Limited. (c) Long-term cycle performance of the Li-S battery/CNF-T interlayer at 1 C [41]. Copyright 2016, American Chemical Society.

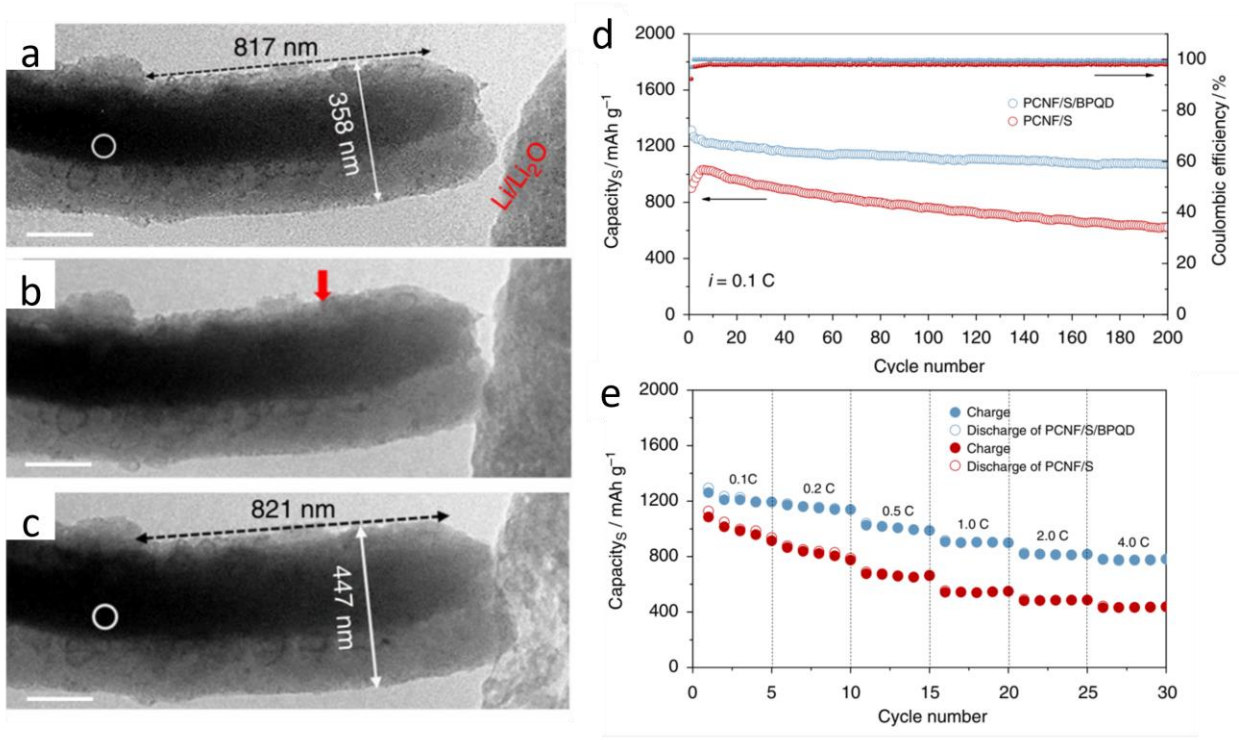

Figure 5. (a, b, c) TEM images of porous carbon nanofibers/sulfur/black phosphorus quantum dots during lithiation. (d) cyclic capacities at 0.1C for 200 cycles and (e) rate capacities from 0.1C to 4C for of porous carbon nanofiber/sulfur and porous carbon nanofiber/sulfur/ phosphorus quantum dots electrodes [46]. Copyright 2018, Springer Nature.

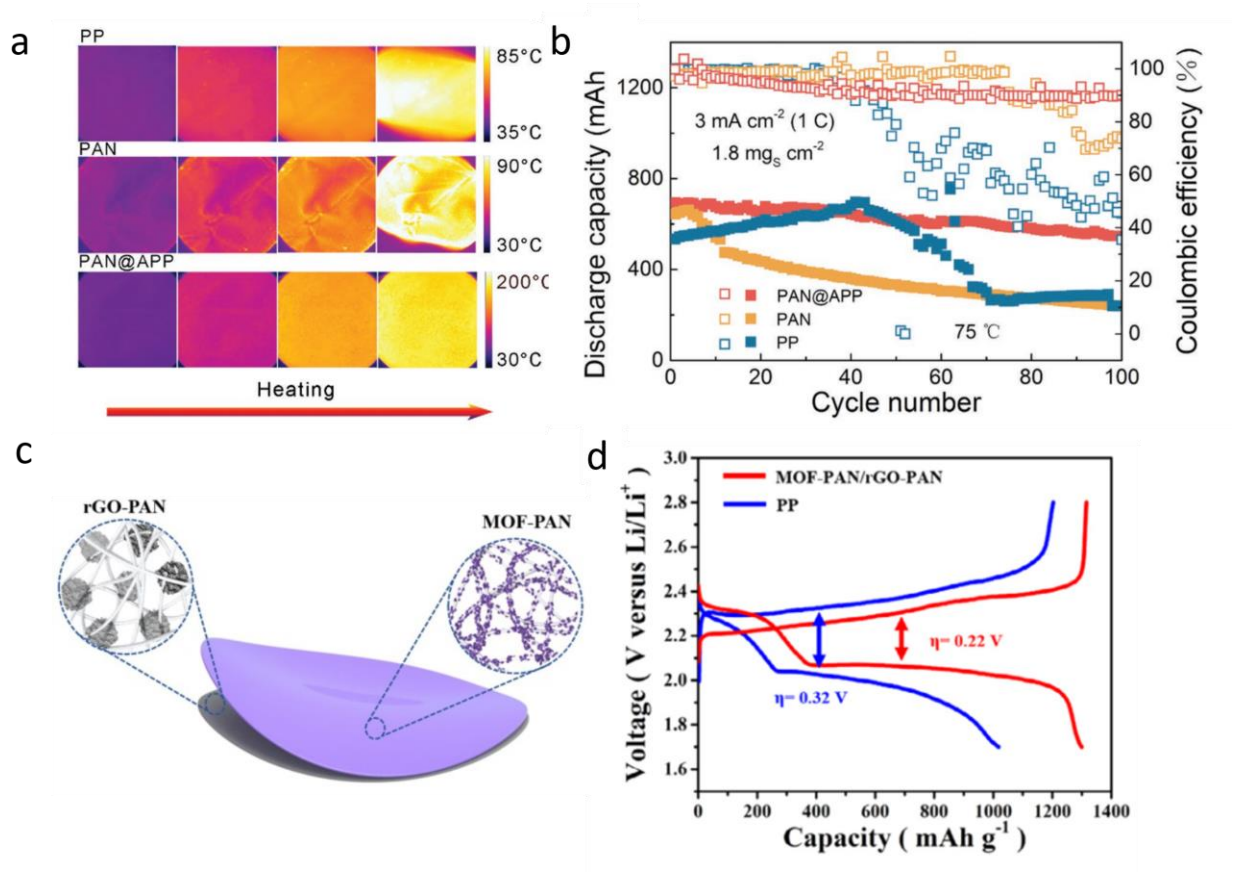

Figure 6 (a) Average thermograms of PP, PAN, and PAN@APP separators, (b) the electrochemistry performance comparison of separators at 75 ℃ [28]. Copyright 2018, WILEY-VCH. (c) Schematic configuration of rGO-PAN/MOF-PAN separator, (d) the electrochemistry performance of LSBs with PP and MOF-PAN/rGO-PAN separators [73]. Copyright 2020, Elsevier.

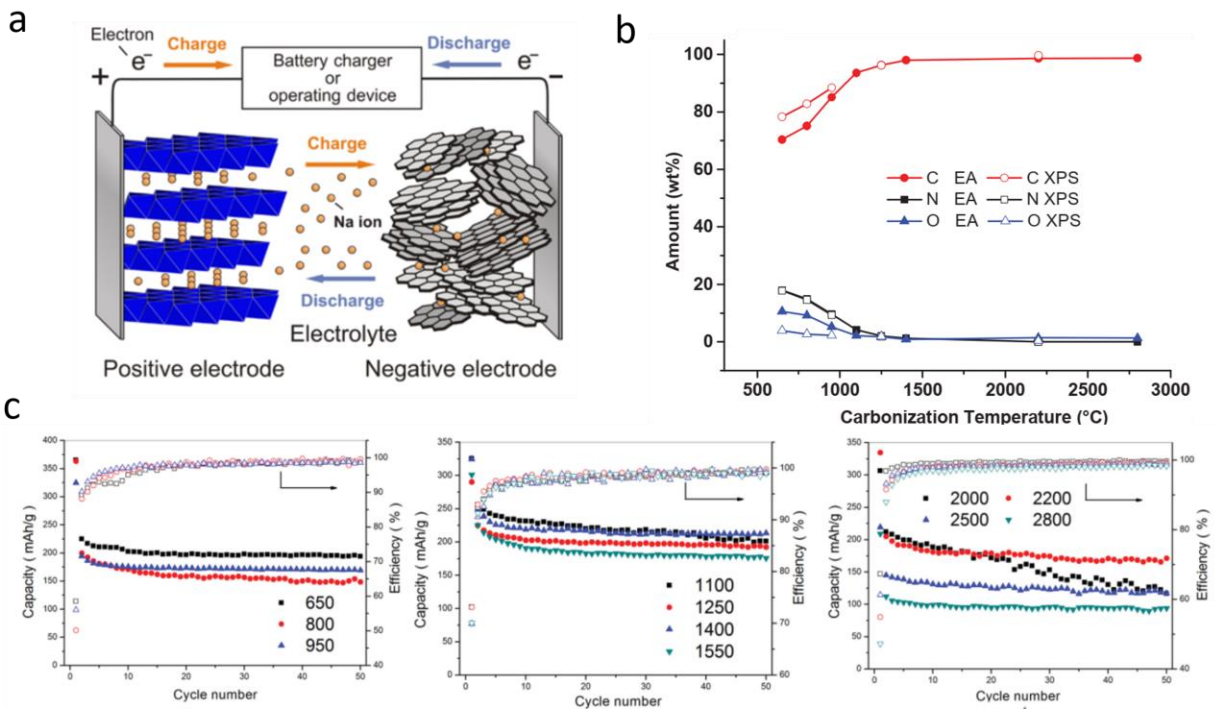

Figure 7 (a) Schematic illustration of Na-ion batteries [5]. Copyright 2014, American Chemical Society. (b) Element composition of carbon nanofibers at different carbonization temperature. (c) electrochemistry of carbon nanofibers anodes anealed at different temperatures [86]. Copyright 2016, WILEY-VCH.

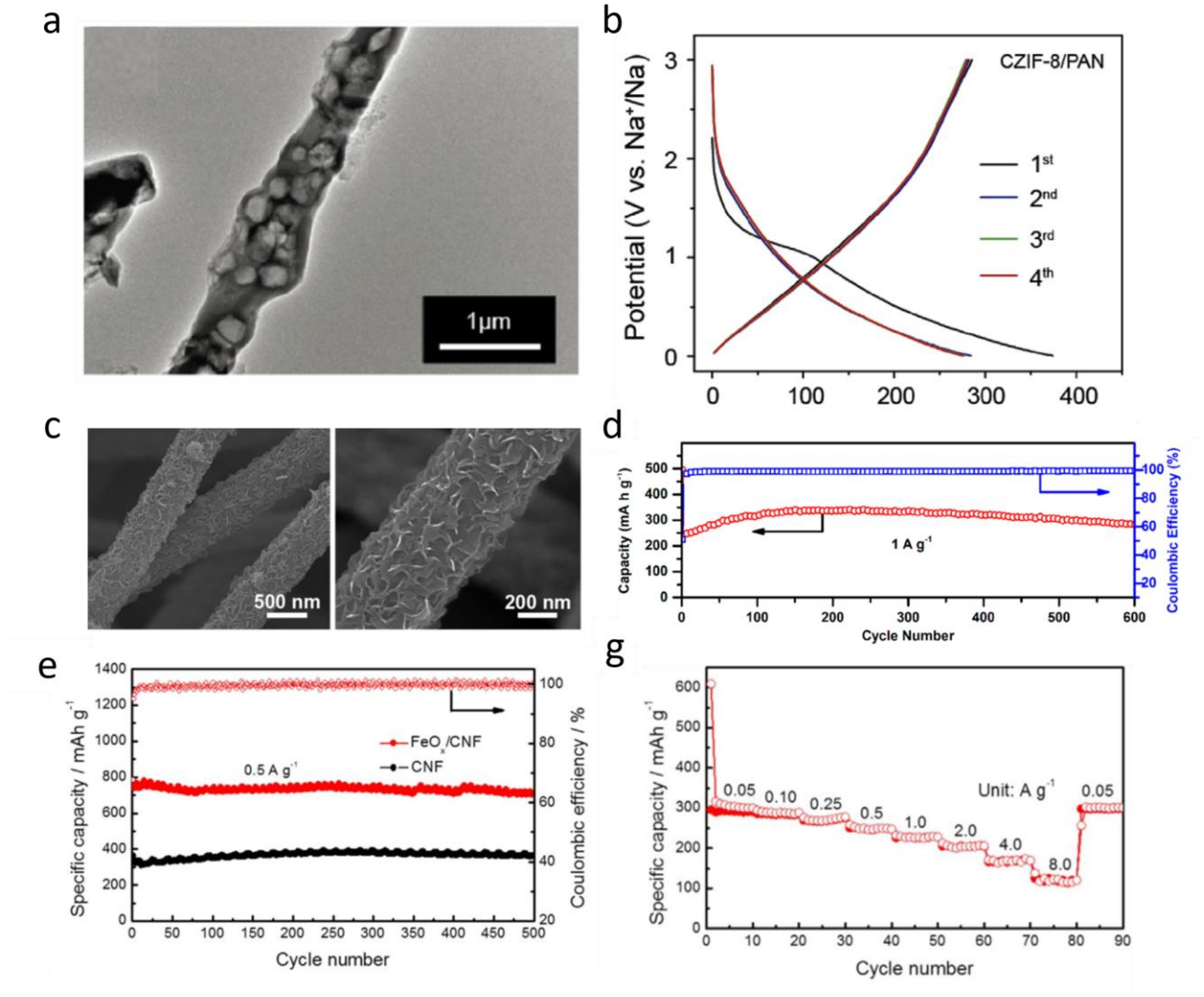

Figure 8 (a) TEM image of CZIF-8/PAN fibers, (b) reversible capacity of CZIF-8/PAN fibers anode in SIBs [89]. Copyright 2020, Elsevier. (c) SEM image of MoS_2 @CNFs and (d) cyclic capacities and Coulombic efficiencies of MoS_2@CNFs anodes in SIBs at 1 A g^{-1} [81]. Copyright 2018, American Chemical Society. (e, g) Cycle and rate performance of FeO_x/CNF anodes in SIBs [32]. Copyright 2017, Elsevier.

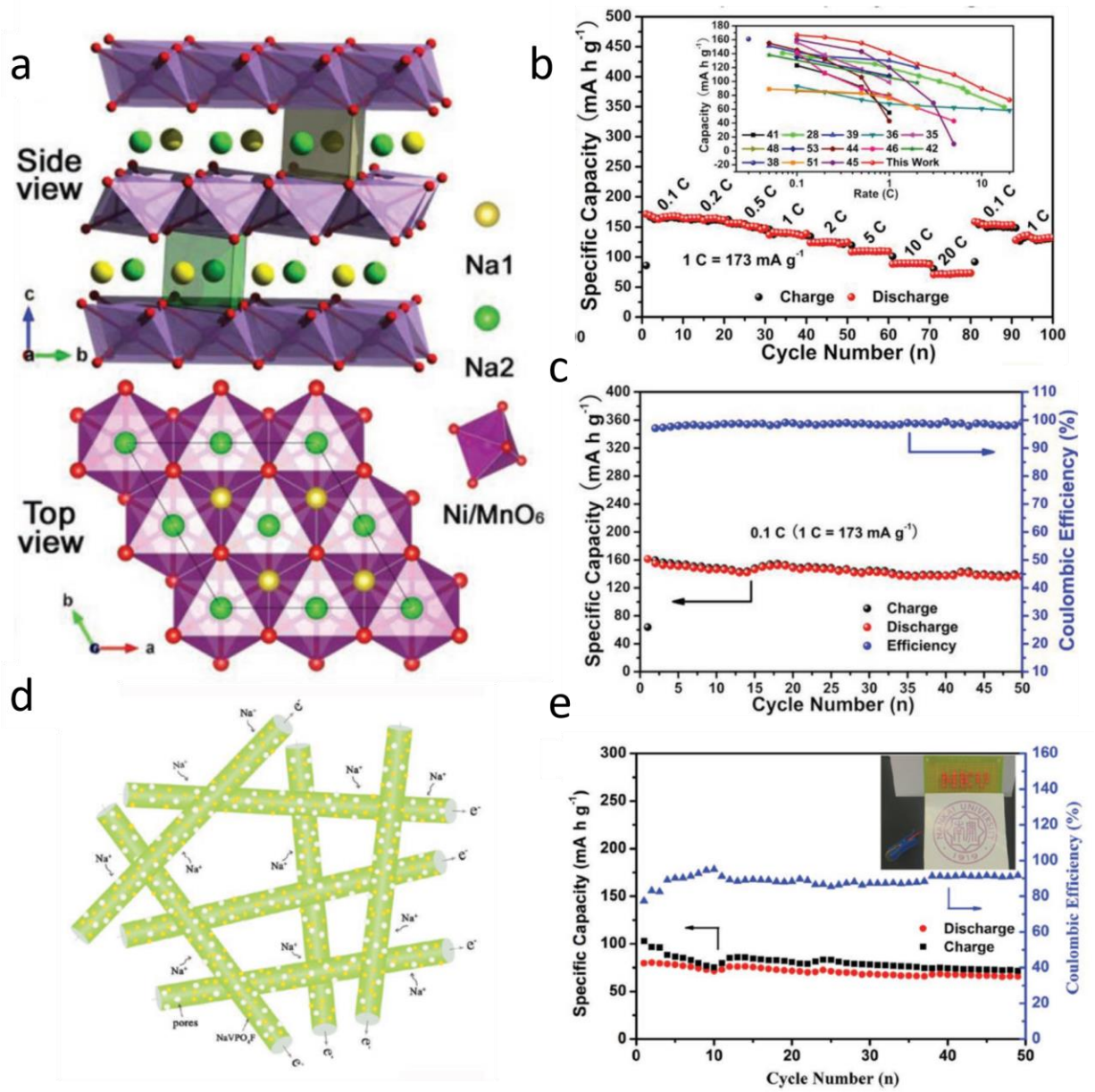

Figure 9 (a) Schematic illustration of the P2-type crystal structure and (b) rate performance of P2-$Na_{2/3}Ni_{1/3}Mn_{2/3}O_2$ nanofibers cathode in SIBs, (c) cycling performance of P2-$Na_{2/3}Ni_{1/3}Mn_{2/3}O_2$//hard carbon full battery at 0.1 C [94]. Copyright 2019, WILEY-VCH. (d) Schematic illustration of $NaVPO_4F$/carbon nanofibers and (e) cycle performance of $NaTi_2(PO_4)_3$ (anode)//$NaVPO_4F$/C (cathode) full battery [96]. Copyright 2017, WILEY-VCH.

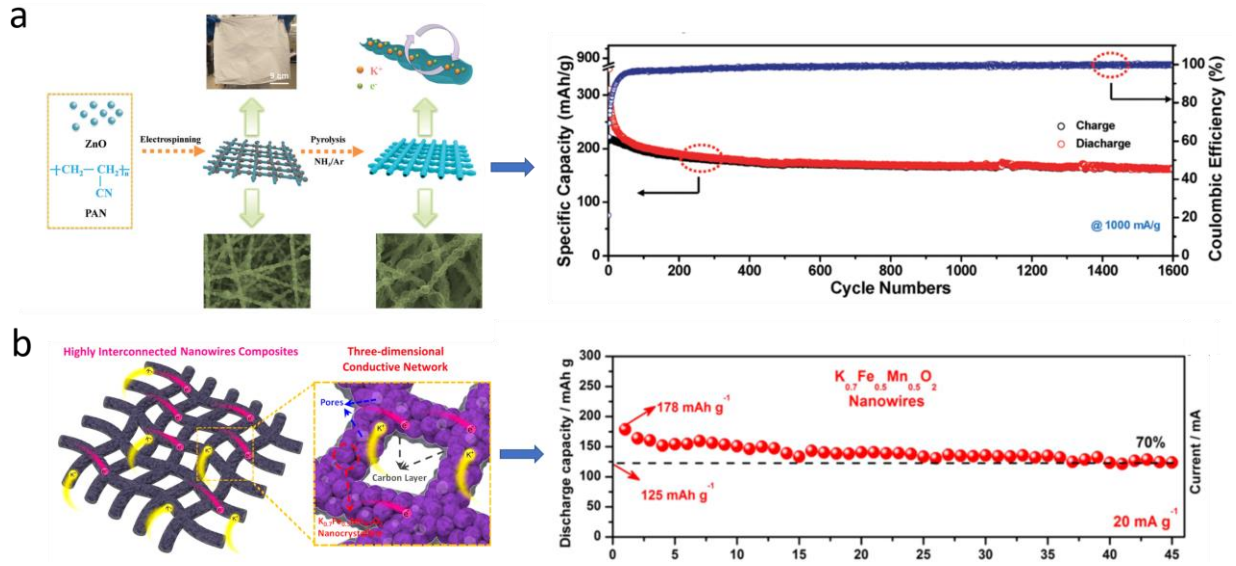

Figure 10 (a) Preparation of freestanding ecklace-like N-doped hollow carbon with hierarchical pores and the anode cycling performance in KIBs [107]. Copyright 2019, the Royal Society of Chemistry (b) $K_{0.7}Fe_{0.5}Mn_{0.5}O_2$ nanowires 3D network and the electrochemical performance in KIBs [118]. Copyright 2016, American Chemical Society.

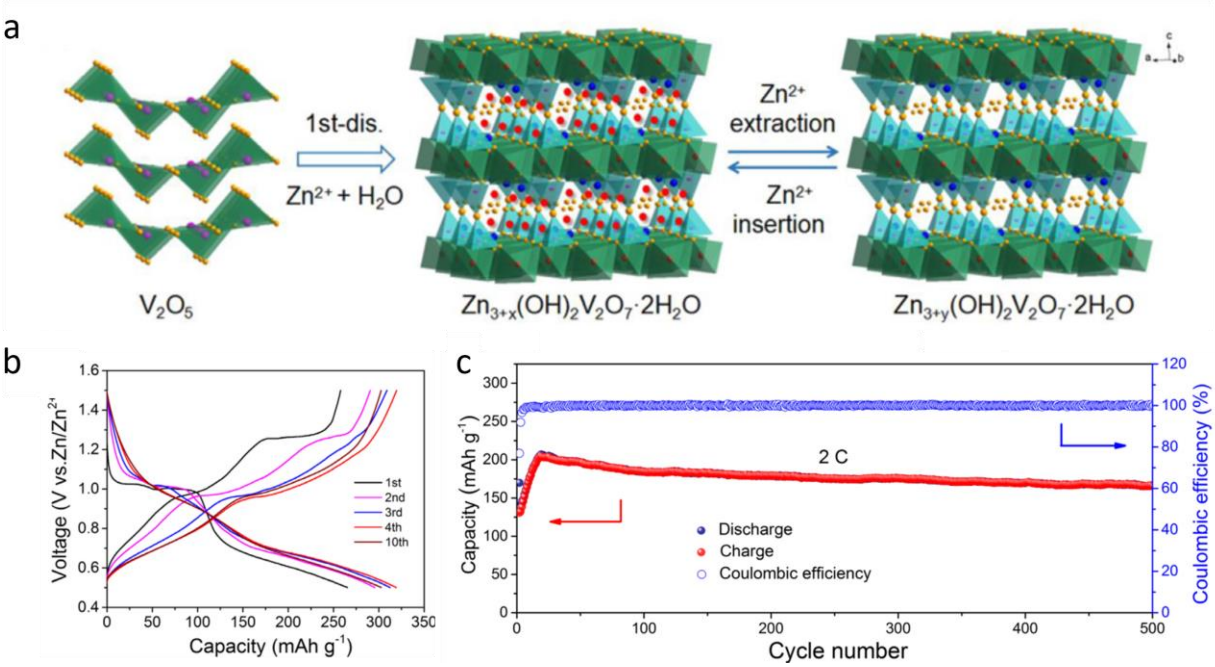

Figure 11 (a) Reaction mechanism of V_2O_5 nanofiber cathode in aqeous ZIBs. (b, c) electrochemical performance of V_2O_5 cathode in ZIBs [120]. Copyright 2019, Elsevier.

Table 1 Comparation abundance in the earth crust, voltage vs. SHE, voltage vs. Li^+/Li, gravimetric capacity, volumetric capacity, Shannon's ionic radius, relative atomic mass, mass to electro ration, dendrite-free of Li, Na, Mg, Al, K, Zn [5, 11, 12]

	Abundance / ppm	Voltage vs. SHE / V	Voltage vs.Li^+/Li / V	Specific capacity / mAh g^{-1}	Volumetric capacity / mAh cm^{-3}	Shannon's ionic radius / Å	Relative atomic mass	Dendrite-free
Li	20	-3.04	0	3861	2062	0.76	6.94	no
Na	23600	-2.71	0.33	1166	1131	1.02	22.98	no
Mg	950	-1.55	1.49	2205	3837	0.72	24.31	yes
Al	82300	-1.66	1.38	2980	8046	0.535	26.98	yes
K	20900	-2.93	0.11	685	591	1.38	39.1	no
Zn	70	-0.76	2.28	820	5855	0.74	65.39	no

Table 2 Electrochemical performance of representative electrospun nanofiber materials in post-lithium ion batteries

Post-Li ion batteries	Materials	Electrospinning solution (precursor/ polymer/solvent)	Specific capacity (mAh g^{-1})/cycle	Cyclability (cycles/capacity retention)	Rate Capability (mAh g^{-1})	Ref
LSBs (Cathode)	Porous CNFs	-/PAN, PMMA/DMF	1400 at 0.05C /1st	30/85% at 0.05C	1400 at 0.05C, 1100 at 0.1C, 900 at 0.2C	[33]
	Activated multichannel CNFs	-/PAN, PMMA/DMF	1351 at 0.2C/ 1st	300/79% at 0.2C	847 at 5C	[44]
	Hierarchical porous CNFs	SiO_2/PAN/DMF	1070.6 at 0.5C/1st	100/88.4% at 0.5C	1318.2 at 0.1C, 1175.6 at 0.2C, 748.6 at 1C, 626.6 at 2C	[17]
	Porous CNFs	$Fe(acac)_3$/PAN/DMF	945 at 1 C/1st	100/81% at 1C	906 at 0.3C, 799 at 1.0C, 742 at 1.5C, 697 at 2C	[29]
	Porous hollow CNTs/CNFs	$Ni(Ac)_2{\cdot}4H_2O$ /PMMA,PAN/DMF	1313 at 0.2C/2nd	100/~79.8% at 1C, 100/~74.8% at 5C	1078 at 0.5C, 878 at 1C, 572 at 5C	[15]
	Porous CNFs/CNT	MWCNTs/PAN/ DMF	1592 at 0.05A g^{-1} /1st	100/637 mAh g^{-1} at 0.05A g^{-1}	645 at 0.1A g^{-1}, 575 at 0.2A g^{-1}, 500 at 0.5A g^{-1}, 437 at 1A g^{-1}	[52]
	rGO/Porous CNF	-/PAN, PMMA/DMF	801.9 at 0.1C/1st	52~200/88% at 0.1C	~690 at 0.2C, ~620 at 0.3C	[56]
	N-doped porous CNFs	-/PTFE, PVP/DI water	1093.9 at 0.5C/1st	300/76% at 0.5C	866.5 at 1C, 731.2 at 2C	[58]
	TiO_2 NFs	$Ti(C_4H_9O)_4$, CH_3COOH/PVP/ C_2H_5OH	~920 at 0.335A g^{-1} /1st	50/58% at 0.335A g^{-1}	357 at 1A g^{-1}	[59]

	BPQD/porous CNF	$Fe(acac)_3$ /PAN/DMF	1234 at 0.1C/1st	200/86.8 % at 0.5C	1030 at 0.5C, 821 at 2C, 784 at 4C	[46]
	S/C/PAN NFs	S/C composite /PAN/DMF	1179 at 0.2A g^{-1} /1st	400/60% at 4A g^{-1}	676 at 3A g^{-1}, 616 at 4A g^{-1}	[60]
	S/DPAN/KB NFs	S/KB composite PAN/DMF	1128 at 0.1C/2nd	150/917 mAh g^{-1} at 0.1C	977 at 0.2C, 483 at 0.5C, 342 at 1C	[61]
	Nafion Nanoweb	Nafion/PVP/ethanol	1056 at 0.5C/-	200/65.8%	~650 at 1C, ~430at 2C	[62]
LSBs (Interlayer)	Porous CNFs/S	-/PAN/DMF	1549 at 0.2C/1st	100/83% at 0.2C	1297.9 at 1C	[65]
	Fe_3C/CNFs	$Fe(acac)_3$ /PAN/DMF	1177 at 0.2 A g^{-1} /1st	100/76% at 0.2A g^{-1}	~780 at 1A g^{-1}, ~690 at 2A g^{-1}	[31]
	TiO_2/CNFs	-/PAN/DMF	1328 at 0.2C /1st, 935 at 1C/1st	500/74.2% at 1C	940 at 0.5C, 740 at 1 C, 620 at 2C	[41]
	MoO_2/CNFs	H_3PO_4, MoO_3/PAN/DMF	1366 at 0.42 mA cm^{-2} /1st	150/73.6% at 0.42 mA cm^{-2}	1250 at 0.84 mA cm^{-2}, 1100 at 2.1 mA cm^{-2}, 970 at 4.2 mA cm^{-2}	[69]
LSBs (Electrolyte)	PAN/PMMA NFs	-/PAN,PMMA/DMF	1200 at 0.15 mA cm^{-2} /1st	50/~63.3% at 0.15 mA cm^{-2}	-	[70]
LSBs (Separator)	PAN@APP	-/PAN,APP/DMF	1270 at 0.2C/1st	100/88% at 0.2C	815 at 1C, 631 at 2C, 507 at 3C	[28]
	E-PAN/PAA NFs	-/PAN,PAA/DMF	1232 at 0.1C/1st, 641 at 1C/1st	500/85.6% at 1C	750 at 1C, 675 at 2C, 624 at 3C	[63]
	MOF-PAN/rGO-PAN	$Co(acac)_2$/PAN/DMF, GO/PAN/DMF	1302 at 0.5C/1st	600/82% at 6C	909 at 2C, 745 at 3C, 485 at 5C	[73]

SIBs (Anode)	Hollow CNFs	-/PMMA/DMF	326 at 0.02A g^{-1}/1st	5000/70% at 1.6A g^{-1}	85 at 1.6A g^{-1}	[30]
	CZIF-8/PAN	ZIF-8/PAN/DMF	374.2 at 0.05A g^{-1} /1st	600/93.5% at 1 A g^{-1}	188.0 at 1A g^{-1}, 169.8 at 2A g^{-1}, 153.0 at 5A g^{-1}	[89]
	MoS_2/CNFs	-/PAN/DMF	528 at 0.1A g^{-1}/1st	100/83% at 0.1 A g^{-1}, 600/ ~100% at 1A g^{-1}	412 at 1A g^{-1}	[81]
	MoS_2/CNFs/G	-/ODA, PMDA/DMAc	598 at 0.1A g^{-1} /1st, 478 at 1A g^{-1}/1st	1000/86.2% at 1A g^{-1}	98.0 at 1A g^{-1}, 477 at 2A g^{-1}, 456 A g^{-1} at 5A g^{-1}	[82]
	TiO_2/C	$Ti(OC_4H_9)_4$/PVP/ ethanol, acetic acid	~260 at 0.2C/1st	500/92.8% at 0.5C, 500/94% at 10C	200 at 10C	[91]
	FeO_x/CNF	$C_{10}H_{16}FeO_4$ /PAN/DMF	~320 at 0.5A g^{-1}/2nd	500/~100%	169 at 4A g^{-1}, 124 at 8A g^{-1}	[32]
SIBs (Cathode)	$Na_{2/3}Ni_{1/3}Mn_{2/3}O_2$ NFs	$Mn(CH_3COO)_2{\cdot}4H_2O$,$NaNO_3$,$Ni(NO_3)_2{\cdot}6H_2O$,$CH_3COOH$ /PVP/DI water,	172 at 0.1C/1st	500/~81% at 5C	166.7 at 0.1C, 89.6 at 10C, 73.4 at 20C	[94]
	$NaCrO_2$ NWs	$NaNO_3$,$Cr(NO_3)_3{\cdot}9H_2O$/PVP/ DI water	122.6 at 0.1C/1st	300/88.4% at 2C	108.8 at 10C, 87.2 at 50C	[95]
	$NaVPO_4F$/CNFs	NH_4VO_3, $NH_4H_2PO_4$,NaF, $H_2C_2O_4{\cdot}2H_2O$/PVP/DI water	126.3 at 1C/1st	1000/96.5% at 2C	61.2 at 50C	[96]
	Na_2FePO_4F/CNFs	Citric acid, $Fe(CH_3COO)_2$,NaH_2PO_4,NaF /PVP/DI water	~117.8 at 0.1C/1st	2000/85% at 5C	46.4 at 20 C	[97]
	Poly(5-cyanoindole) nanofiber	-/poly(5 cyanoindole)/acetonitrile	97 at 0.2C/1st, 106 at 0.2C/8th	400/96.2%, 94.6%, 92.7% at 0.2C,1C, 2C	102 at 1C, 75 at 10C	[101]
PIBs (Anode)	Porous CNFs	-/PAN, PMMA/DMF	270 at 0.02A/80th	1200/88% 0.2A g^{-1}	190 at 2A g^{-1}, 140 at 5 A g^{-1}, 100 at 7.7 A g^{-1}	[106]
	N-doped necklace-like	ZnO/PAN/DMF	~315 at 0.1 A g^{-1}/20th	20~1000/90% at 0.2A g^{-1}	204.8 at 2 A g^{-1}	[107]

	hollow carbon CNF					
	Highly graphitized CNFs	-/PAN/DMF	265 at 0.1C/1st	400/96.7% at 0.2C	226 at 35C	[109]
	MoSSe/CNFs	-/PAN/DMF	389.6 at 0.1 A g^{-1}/60th	1000/84.6% at 0.5 Ag^{-1}	250.8 at 2A g^{-1}, 202.6 at 5A g^{-1}	[112]
	Cu_2Se/CNFs	Cu_2O/PAN, PVP/DMF	~190 at 0.1 A g^{-1}/8th	1200/78 mAh g^{-1} at 2A g^{-1}	104 at 2A g^{-1}	[113]
	Sb/Nanochannel CNFs	$Sb(Ac)_3$/PAN,PS/DMF	949 at 0.2A g^{-1}/1st	2000/225 mAh g^{-1} at 1A g^{-1}	237 at 2A g^{-1}, 207 at 5A g^{-1}	[117]
KIBs (Cathode)	SeS_2/N-doped CNFs	-/PAN,PS,Pluronic F127/DMF	~751 at 0.05A g^{-1}/2nd	1000/85% at 0.5A g^{-1}	439 at 1 A g^{-1}, 372 at 2 A g^{-1}	[111]
	$K_{0.7}Fe_{0.5}Mn_{0.5}O_2$	CH_3COOK,$Fe(acac)_3$,$Mn(acac)_3$/PVP/DI water	114 at 0.1A g^{-1} /1st	60/89% at 0.1A g^{-1}	~52 at 1 A g^{-1}	[118]
	Porous V_2O_5 NFs	NH_4VO_3, $H_2C_2O_4{\cdot}2H_2O$/PVP/DMF	319 at 0.02A g^{-1}/4th	500/81% at 0.02A g^{-1}	125 at 8 A g^{-1}, 104 at 10 A g^{-1}	[120]
ZIBs (Cathode)	V_2O_5/CNF, $Zn_2V_2O_7$/CNF	$VO(acac)_2$, CH_3COOH /PAN, PMMA/DMF $Zn_2V_2O_7$ /PMMA,PAN/DMF	~502(V_2O_5/CNF), ~248($Zn_2V_2O_7$/CNF) at 0.1 A g^{-1}/30th	2000/95.8% (V_2O_5/CNF), 93.1%($Zn_2V_2O_7$/CNF) at 8A g^{-1}	409(V_2O_5/CNF) , 162($Zn_2V_2O_7$/CNF) at 8A g^{-1}	[16]
	MnO/N-doped CNFs	$Mn(Ac)_2{\cdot}4H_2O$/PVP/C_2H_5OH	250.1 at 0.1 A g^{-1}/15th	200/ 176.3 mAh g^{-1} at 0.5A g^{-1}	100.5 at 1.2 A g^{-1}, 66.3 at 2 A g^{-1}	[67]
	Mn_3O_4/CNFs	Mn_3O_4/PMMA/DMF	~220 at 0.1 A g^{-1} /5th	1300/ 225 mAh g^{-1} at 0.4A g^{-1}	215.8 at 0.3 A g^{-1}, 115.7 at 2.0 A g^{-1}	[121]
AIBs (Cathode)	$MoSe_2$/N-doped CNFs	-/PAN/DMF	296.3 at 0.1 A g^{-1}/1st	200/169.9 mAh g^{-1} at 0.1A g^{-1}	193.5 at 0.2A g^{-1}, 159.0 at 0.25A g^{-1}	[128]
MIBs (Cathode)	V_2MoO_8	NH_4VO_3, $H_{24}Mo_7N_6O_{24}$/PVP/C_2H_5OH	312 at 0.02 A g^{-1}/1st	50/72.5% at 0.02 A g^{-1}	123.6 at 0.2 A g^{-1}, 190.4 at 0.5 A g^{-1}	[133]